The 8 June 1995 McLean, Texas, Storm. Part II: Cyclic Tornado Formation, Maintenance, and Dissipation

DAVID C. DOWELL*

NOAA/National Severe Storms Laboratory and Cooperative Institute for Mesoscale Meteorological Studies, Norman, Oklahoma

HOWARD B. BLUESTEIN

School of Meteorology, University of Oklahoma, Norman, Oklahoma

(Manuscript received 4 May 2001, in final form 18 April 2002)

ABSTRACT

On 8 June 1995, scientists participating in the Verification of the Origins of Rotation in Tornadoes Experiment (VORTEX) collected a unique dataset with the Electra Doppler Radar (ELDORA). The ELDORA observations document the sequential life cycles of storm-scale circulations associated with three large tornadoes in a supercell thunderstorm near McLean, Texas. A qualitative description of the evolution of the storm was provided in Part I of this paper.

During the first stage of development of each storm-scale circulation, interaction of the updraft with the environmental low-level horizontal vorticity produced a vorticity column that increased in intensity with height. As the vortex matured, vorticity increased greatly at low levels (i.e., below 2 km AGL) and exceeded that aloft. Each tornadic vortex was located near the rear side of the updraft, where the surrounding low-level horizontal vorticity was modified locally, most likely by weak baroclinity within the storm. Tilting of low-level horizontal vorticity into the vertical, followed by stretching of the vertical vorticity, occurred in the air parcels that entered the rear portion of the main storm updraft from its left (as viewed in the direction of storm motion). Although the region of tilting was near the interface of the main updraft and that portion of the downdraft to the left of the updraft, there is no direct evidence in the observations (above 500 m AGL) of generation of cyclonic vertical vorticity by tilting in the downdraft itself.

For this storm, *the cyclic tornadogenesis process was associated with a mismatch between the horizontal motion of successive tornadoes and the horizontal velocity of the main storm-scale updraft and downdraft.* Low-level updraft-relative flow seemed to be the most important factor in determining tornado motion.

1. Introduction

During the Verification of the Origins of Rotation in Tornadoes Experiment (VORTEX) in 1994–95 (Rasmussen et al. 1994), university and government scientists collected datasets to be used for testing hypotheses about tornado formation. In Dowell and Bluestein (2002, Part I of this paper), we described a dataset collected primarily with research aircraft during VORTEX on 8 June 1995. On this date, the Electra Doppler Radar (ELDORA; Hildebrand et al. 1994; Wakimoto et al. 1996) scanned a series of tornadoes as they formed at a range of 5–15 km in a supercell near McLean, Texas. The pseudo-dual-Doppler (Jorgensen et al. 1996; Dowell et al. 1997) wind field syntheses of the ELDORA data resolve features on scales as small as 2–3 km, every 5–6 min, for a period of over 1.5 h.

Before VORTEX, only a few fortuitous multiple-Doppler datasets were available that captured the genesis stage of a tornado (Heymsfield 1978; Brandes 1978, 1981; Ray et al. 1981; Dowell and Bluestein 1997). Some of these datasets collected with ground-based radars at fixed sites match the 8 June 1995 ELDORA dataset in terms of either spatial or temporal resolution, but not both. For example, the Del City storm of 20 May 1977 was relatively close to both radars when the tornado formed, but there are gaps of up to 20 min between dual-Doppler volume scans. The advantage of airborne platforms such as the ELDORA is that one may follow the target storm and scan it at close range for a long period of time.

The McLean storm formed in a supercell environment having high CAPE (over 5000 J kg^{-1}) and strong vertical shear of the horizontal winds [bulk Richardson number (BRN) shear (Weisman and Klemp 1982) of

* Current affiliation: National Center for Atmospheric Research, Boulder, Colorado.

Corresponding author address: David C. Dowell, National Center for Atmospheric Research, P. O. Box 3000, Boulder, CO 80307-3000. E-mail: ddowell@ucar.edu

© 2002 American Meteorological Society

17.5 m s^{-1}]. The fourth of five tornadoes in the storm produced F4/F5 damage and could have been the most intense tornado ever scanned in multiple-Doppler fashion as of the end of VORTEX. Furthermore, the pseudo-dual-Doppler analyses of the McLean supercell are the first to document the cyclic formation at close range of storm-scale circulations associated with large tornadoes.

In Part I of this paper, we described the sequence of events in the analyses of the McLean storm and compared storm features to those in prevailing conceptual models of tornadic storms. The discussion in this part centers around the following dynamical questions: What was the source of rotation at cloud base in the storm-scale (1–3 km wide) circulations associated with the tornadoes? Why did these circulations dissipate? Why did the storm produce a family of tornadoes rather than one tornado? Why was the fourth tornado stronger and longer lived than the other tornadoes? Limitations in resolution preclude a definitive diagnosis down to the scale of the tornado. We therefore focus on the vorticity dynamics of air parcels approaching the storm-scale circulations around the tornadoes and the relationships of the tornadoes to the larger-scale updrafts and downdrafts of the parent storm.

2. The dynamics of mesocyclone and tornado formation, maintenance, and dissipation

a. Background

The equation governing the time rate of change of vertical vorticity is

$$\frac{\partial \zeta}{\partial t} = -\left(u\frac{\partial \zeta}{\partial x} + v\frac{\partial \zeta}{\partial y}\right) - w\frac{\partial \zeta}{\partial z} + \left(\frac{\partial u}{\partial z}\frac{\partial w}{\partial y} - \frac{\partial v}{\partial z}\frac{\partial w}{\partial x}\right) - \delta\zeta + \left[\frac{\partial}{\partial y}\left(\frac{1}{\rho}\right)\frac{\partial p}{\partial x} - \frac{\partial}{\partial x}\left(\frac{1}{\rho}\right)\frac{\partial p}{\partial y}\right] + \left(\frac{\partial F_y}{\partial x} - \frac{\partial F_x}{\partial y}\right), \quad (2.1)$$

where ζ is the vertical component of vorticity, δ is the horizontal divergence, p is the perturbation pressure, ρ is density, F_x and F_y represent the x and y components of turbulent mixing, and u, v, and w, are the zonal, meridional, and vertical components of motion respectively. The terms on the right-hand side of (2.1) represent horizontal advection of vertical vorticity, vertical advection of vertical vorticity, tilting of horizontal vorticity into the vertical, stretching of vertical vorticity, solenoidal generation of vertical vorticity, and frictional generation/dissipation of vertical vorticity, respectively. The solenoidal term is typically neglected based on scale analysis (Heymsfield 1978). In addition, it is usually impossible to evaluate the friction term with observations alone.

We will sometimes also find it convenient to consider macroscopic measures of rotation, rather than point measures, by using the following definition for circulation:

$$C \equiv \oint \mathbf{v} \cdot d\mathbf{l}, \quad (2.2)$$

where the integration is along a counterclockwise closed path and $d\mathbf{l}$ is a length element along the path. In frictionless, barotropic flow, circulation about a material curve is conserved.

For a detailed discussion of the formation of mesocyclones and tornadoes in supercells, we refer the reader to Barnes (1968), Lilly (1982), Klemp (1987), Davies-Jones and Brooks (1993), Walko (1993), Wicker and Wilhelmson (1995), and Adlerman et al. (1999). There is general agreement that the formation aloft of vortices on a horizontal scale of ~5 km in supercells, with vertical vorticity of ~0.01 s^{-1}, is a result of the tilting of horizontal vorticity (associated with the vertical shear of the horizontal wind) into the vertical by the main updraft. We will focus here instead on some of the issues pertaining to tornadoes specifically. How do only relatively few supercells produce intense 100-m-scale rotation near the surface with vertical vorticity on the order of 1.0 s^{-1}?

The common thread in previously posed hypotheses of mechanisms of tornadogenesis is that some process provides vertical vorticity in the boundary layer that subsequently gets amplified by convergence. Perhaps the simplest possible mechanism is that localized vertical vorticity is already present in the storm environment along a preexisting boundary, and the updraft simply stretches this vertical vorticity as it ingests air from along the boundary. Wakimoto and Atkins (1996) suggest that this conceptual model for nonsupercell tornadogenesis (Brady and Szoke 1989; Wakimoto and Wilson 1989) could also apply to some supercells.

Many hypotheses for the formation of intense vortices involve a two-step process: tilting of horizontal vorticity into the vertical, followed by stretching of the vertical vorticity (e.g., Klemp and Rotunno 1983; Davies-Jones and Brooks 1993; Wicker and Wilhelmson 1995). Among the tilting–stretching theories, there are differences in the nature of the horizontal vorticity that is tilted and the vertical motion field that does the tilting. In perhaps the most widely cited hypothesis for the formation of strong low-level vortices in supercells, tilting of baroclinically generated horizontal vorticity into the vertical by the updraft and stretching of vertical vorticity within the updraft produce the low-level vortex (Rotunno and Klemp 1985). The horizontal vorticity develops in air parcels that approach the low-level updraft from the forward-flank baroclinic zone at the edge of the pool of rain-cooled air.

Since air parcels move away from the surface as they acquire vertical vorticity from tilting and stretching in an updraft, Davies-Jones and Brooks (1993) and Walko (1993) questioned whether an updraft-only process could produce strong rotation within a few hundred meters of the surface. Instead, they stressed the importance

of the vertical velocity gradient within a *downdraft* in tilting horizontal vorticity into the vertical. In the Davies-Jones and Brooks (1993) simulation, the tilting occurred in that portion of the rear-flank downdraft (Lemon and Doswell 1979) to the left of the low-level updraft (where directions described are relative to a viewer looking in the direction toward which the parent storm is moving). The weak vertical vorticity in this region was subsequently amplified by convergence in air parcels entering the roots of the low-level updraft from the left-rear side. Although the mechanism of low-level vortex formation appears to be quite similar to that in the Rotunno and Klemp (1985) simulation, Rotunno and Klemp did not discuss the process of tilting in descending air.

In a numerical simulation of low-level vortex formation by Walko (1993), *environmental* horizontal vorticity (i.e., horizontal vorticity associated with vertical shear of the horizontal wind in the basic state), rather than baroclinically generated horizontal vorticity, was tilted into the vertical. As in the Davies-Jones and Brooks (1993) simulation, air parcels acquired vertical vorticity by tilting in a downdraft followed by stretching in an updraft. However, local baroclinic generation of horizontal vorticity was not necessary, and it even acted to oppose the formation of the vortex. Much earlier, the association of tornadic supercells with environments having strong vertical shear of the horizontal wind led to speculation that tornadoes derive their rotation from this environmental shear (Browning and Landry 1963; Barnes 1968). The results from thunderstorm simulations later by Wicker (1996) suggested that environmental vertical shear very close to the surface may be as important for low-level vortex formation as local baroclinic generation of horizontal vorticity.

Tornado maintenance requires a continued collocation of vertical vorticity and horizontal convergence. The low pressure of the tornado itself helps to sustain the convergence by accelerating parcels inward in a shallow layer near the surface where friction leads to an imbalance of the pressure gradient and centrifugal forces (e.g., as reviewed by Lewellen 1993). With radial inflow at the bottom, vortex steadiness requires a mechanism for lifting air out of the boundary layer. At low levels, an upward-directed perturbation pressure gradient force could accomplish this (Leslie 1971; Wicker and Wilhelmson 1995; Trapp and Davies-Jones 1997). However, at some level, positive buoyancy must ultimately continue to drive the upward exhaust.

A tornado may dissipate if the circulation in the low-level inflow from the surroundings decreases or if the convergence at the base of the updraft decreases. The traditional explanation is the latter; that is, low-level convergence decreases when outflow surrounds the vortex and cuts off the supply of warm environmental air to the updraft (Lemon and Doswell 1979; Brandes 1981; Klemp 1987; Adlerman et al. 1999).

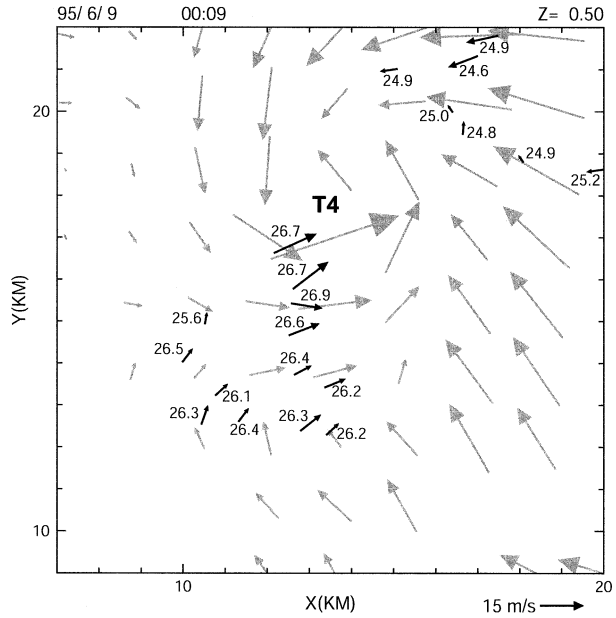

FIG. 1. Mobile-mesonet observations at 3 m AGL (temperatures in °C, horizontal ground-relative winds depicted by black vectors) and horizontal ground-relative winds at 500 m AGL (gray vectors, every fourth vector plotted) in the pseudo-dual-Doppler analysis of ELDORA data. The mobile-mesonet (ELDORA) data were collected between 0015 and 0019 (0007 and 0010) UTC 9 Jun 1995. The location of tornado 4 is labeled T4. The locations of the mobile-mesonet observations are relative to the tornado, which was moving at ($U = 7$ m s^{-1}, $V = 8$ m s^{-1}). The x and y distances (in km) are with respect to the grid origin at McLean, TX.

b. Limitations of the observations

Evidence from numerical simulations suggests that the characteristics of the wind field within a few hundred meters of the ground are the most critical for the development of tornadic rotation (Rotunno and Klemp 1985; Wicker 1996). Unfortunately, the diagnosis of processes near the surface with the airborne radar is not possible, owing to the contamination of low-level data by ground clutter. The depth of the ground clutter is a function of range. In the more distant scans (range ~15 km) of the tornadoes in the McLean storm by the ELDORA, data up to ~500 m AGL are contaminated. A comparison of measurements from multiple sensors reveals evidence of significant vertical gradients of the horizontal wind in the lowest 500 m. For example, the mobile mesonet (Straka et al. 1996) sampled the winds at 3 m AGL around tornado 4 late in the lifetime of the tornado. A comparison of these wind measurements at 3 m AGL and the synthesized ELDORA winds at 500 m AGL indicates generally much weaker winds at the lower level (Fig. 1). [Since the last pass by the Electra at 0015 UTC (hereafter, all times shown are in UTC) was incomplete, we show the results of the synthesis from the previous pass at 0009 in Fig. 1. The wind field at 0015 at locations where data were available near the tornado (not shown) was similar to the wind field during

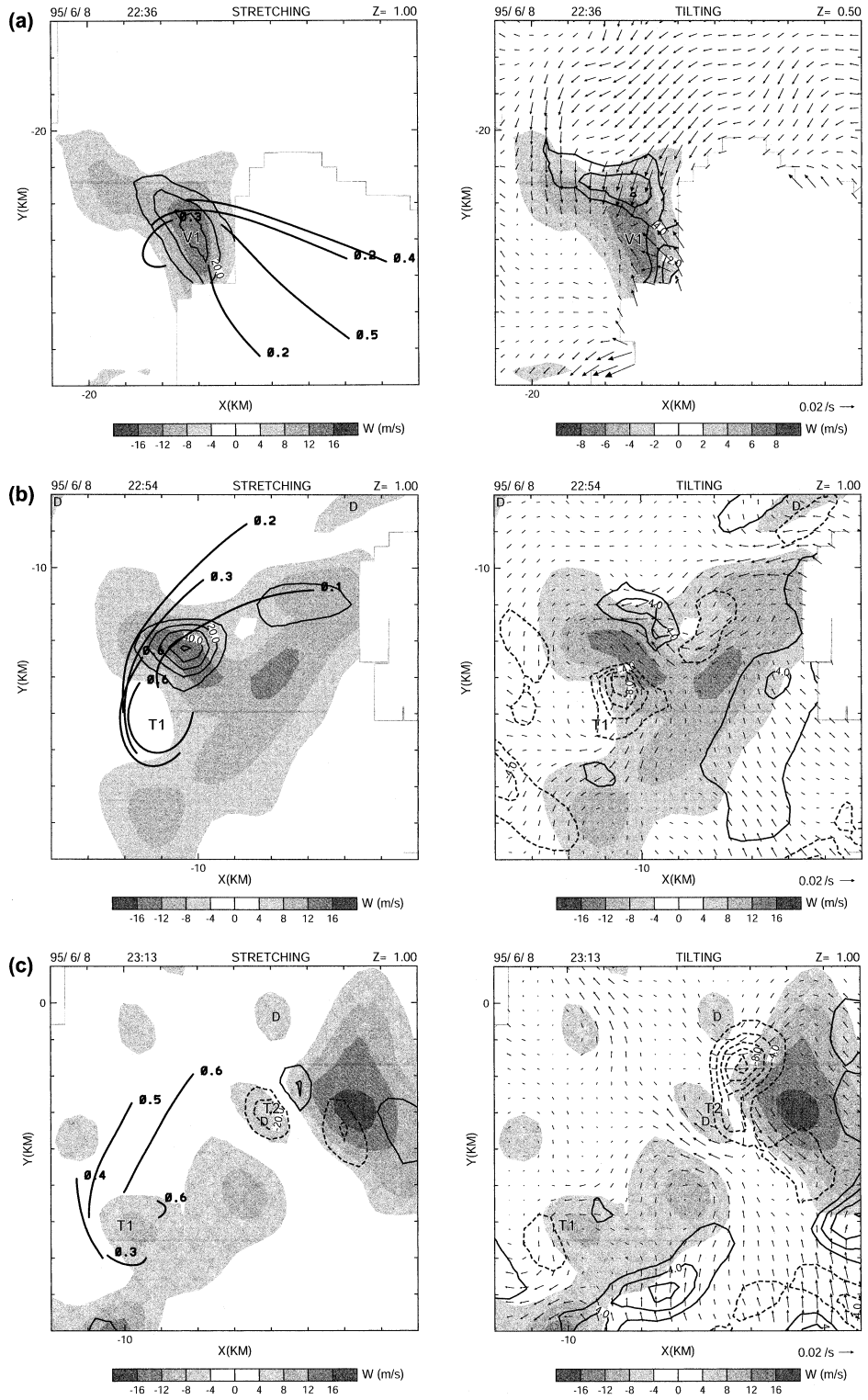
(a)
95/ 6/ 8 22:36 STRETCHING Z= 1.00
95/ 6/ 8 22:36 TILTING Z= 0.50
(b)
95/ 6/ 8 22:54 STRETCHING Z= 1.00
95/ 6/ 8 22:54 TILTING Z= 1.00
(c)
95/ 6/ 8 23:13 STRETCHING Z= 1.00
95/ 6/ 8 23:13 TILTING Z= 1.00
Y(KM)
X(KM)
W (m/s)
-16 -12 -8 -4 0 4 8 12 16
-8 -6 -4 -2 0 2 4 6 8
0.02 /s
V1
T1
T2
D

the previous pass; therefore, the comparison of observations, which are separated by as much as 10 min, is probably still valid.] Ground-clutter contamination of the low-level data particularly makes it difficult to diagnose horizontal vorticity and tilting of horizontal vorticity into the vertical near the surface.

In the environment to the southeast of the updraft of the McLean storm, the direction of the vertical shear vector (and the orientation of the associated horizontal vorticity) veered with height up to nearly 2 km AGL (Fig. 6b in Part I). The wind at 50 m AGL was from the southeast and was considerably stronger than the southeasterly wind observed by the mobile mesonet at 3 m AGL. Within the lowest 50 m, the vertical shear vector (horizontal vorticity) pointed toward the northwest (southwest). Since the direction of storm motion was approximately perpendicular to the direction of the vertical shear near the surface, the horizontal vorticity in the surface layer was approximately streamwise. Higher up, the orientation of the vertical shear (horizontal vorticity) veered around to northeastward (northwestward) at 500 m and eastward (northward) at 1000 m.

Tilting of horizontal vorticity into the vertical can produce vertical vorticity of comparable magnitude to the original horizontal vorticity [$\sim$0.01 s^{-1} at low levels near the McLean storm updraft (e.g., Fig. 2)]. We suppose for the moment that tilting is the dominant process that produces low-level rotation about a vertical axis. For a typical strong tornado (radius $\sim$100 m, vertical vorticity $\sim$1 s^{-1}, and circulation of $\pi \times 10^4$ m^2 s^{-1}) (cf. Fig. 7a in Part I), we would anticipate, by conservation of circulation, that the region of tilting must be relatively broad (at least 2000 m across) in order to produce sufficient total circulation. Although this size is comparable to the smallest resolved scale in the dual-Doppler analyses, it is still difficult to diagnose the tilting process with observations because it is necessary to determine accurate vertical velocities and to resolve sharp vertical gradients in horizontal wind.

After synthesizing the wind fields in the McLean storm, we used centered horizontal and vertical finite differencing to calculate the horizontal vorticity. For the analyses of horizontal vorticity at 1.0 km AGL (e.g., Figs. 2b and 2c), the computation of the vertical shear component was over the layer from 500 m (the approximate height of the lowest uncontaminated Doppler data) to 1500 m AGL. Since we originally analyzed the entire ELDORA dataset with the same wind synthesis method in order to permit unambiguous comparison among different volumes of the several-kilometer-scale features, we did not take advantage of some of the high-resolution raw data obtained at low levels during close aircraft passes. During the first two and the last seven aircraft passes, when the radar was very close to (within 10 km of) the tornado/vorticity maximum, the ground clutter in and near the tornado extended up to only $\sim$300 m AGL. In order to resolve the vertical shear as close to the ground as possible, we produced additional analyses of the data from the close passes. For the analyses of horizontal vorticity below 1 km (e.g., Fig. 2a), we used a 200-m Cressman (1959) vertical radius of influence for the objective analyses of Doppler velocity and synthesized the wind fields on Cartesian grids with a 200-m vertical grid spacing. (The horizontal radius of influence was 800 m, as in the original analyses.) The centered-difference calculations of horizontal vorticity at 500 m AGL (Fig. 2a) involved synthesized winds as low as 300 m AGL.

For the computation of air parcel trajectories (e.g., Fig. 2), we employed linear interpolation in time between consecutive Doppler analyses and trilinear interpolation in space (Ziegler et al. 2001). The trajectories, which end in a 2-km-wide circle around the tornado/vorticity maximum at 1 km AGL, are plotted in a vortex-relative reference frame. Trajectories within data-void regions are based on hole-filled Cartesian velocity components that satisfy the 2D (horizontal) Laplace equations (Ellis 1997). For trajectories originating at very low levels, we assumed the horizontal wind was constant below 500 m. Other reasonable assumptions for the flow below 500 m (not shown) did not change the qualitative interpretation of the trajectories. Since a number of assumptions were involved in the computation of trajectories, we do not trust relatively small-scale details in the analyses of trajectories.

Owing to the limitations of the observations described above, it is not possible to evaluate terms in the vorticity equation along trajectories (or to evaluate conservation of circulation following material curves), as would be required in a definitive demonstration of how a vortex forms. Nevertheless, the analyses of the trajectories and the tendency terms in the vorticity equation do provide clues about the formation, maintenance, and dissipation of the storm-scale circulations. Our assumption in the presentation below is that a significant portion of the angular momentum in each of the three large tornadoes

←

FIG. 2. Stretching of vertical vorticity at 1.0 km AGL (contours, left), tilting of horizontal vorticity into the vertical (contours, right), and vertical velocity (shading, downdrafts labeled with a D). Storm-relative parcel trajectories (dark lines, beginning heights in km) followed backward for 300 s from the tornado/vorticity maximum at 1.0 km are indicated in the plots of stretching. The procedure for determining trajectories within regions of missing data is described in the text; horizontal winds below 500 m AGL are assumed to be identical to those at 500 m. Horizontal vorticity vectors are shown in the plots of tilting. The contour intervals are 10×10^{-5} s^{-2} (stretching) and 2 or 4×10^{-5} s^{-2} (tilting). Tornado 1, the pretornadic vorticity maximum of tornado 1, tornado 2, and the pretornadic vorticity maximum of tornado 2 are labeled T1, V1, T2, and V2, respectively: (a) stretching and tilting (0.5 km AGL) at 2236 UTC, (b) stretching and tilting (1.0 km AGL) at 2254 UTC, and (c) stretching and tilting (1.0 km AGL) at 2313 UTC.

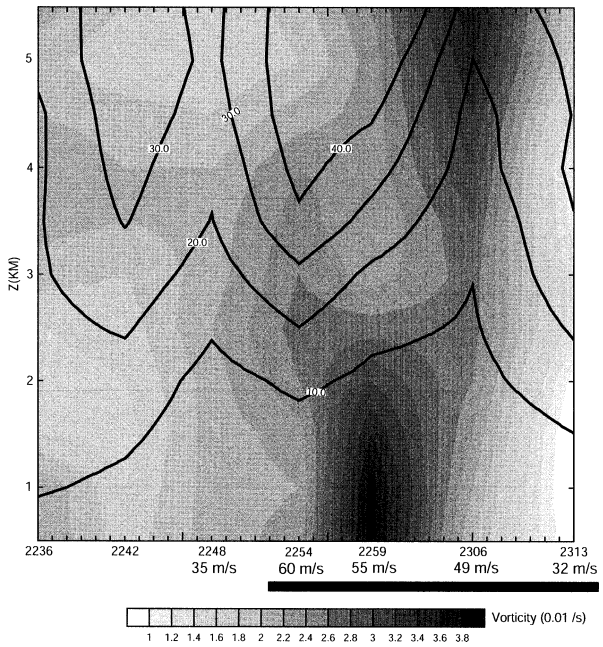

FIG. 3. Objective analysis of mean vertical vorticity (shading, units of 0.01 s^{-1}) and vertical velocity (contours at intervals of 10 m s^{-1}) as a function of height and time in the vortex associated with tornado 1. At each level, the averaging is over a circle of radius 1 km that encompasses the maximum circulation. In order to ensure vertical continuity of the features, the horizontal location of the circle at a particular analysis level is constrained to be within 1 km of its location at the level 500 m below. The times (UTC) of the Doppler analyses are shown at the bottom of the panel. The bar indicates the time period when a condensation funnel was visible. Maximum ground-relative winds below 2 km AGL in the tornado signatures in the raw single-Doppler data are also indicated at the bottom of the panel.

was produced first as rotation about a vertical axis on resolved (i.e., 2 km wide or wider) scales.

c. The life cycle of the first storm-scale circulation

The reader is referred to Figs. 2, 3, and 4 in the following discussion. In this paper, we focus on only tornadoes 1, 2, and 4 in the McLean storm. The other tornadoes (3 and 5) were brief (Fig. 3 in Part I) and rated F0 [winds of 18–32 m s^{-1} on the Fujita (1981) scale]. There is no direct evidence of tornadoes 3 and 5 in the ELDORA data, apparently because they were too narrow to resolve and/or occurred in between Electra scan times. The condensation funnel of the first tornado formed at approximately 2252 on 8 Jun 1995 and dissipated at 2315. Tornado 1 caused F2 damage (NCDC 1995); low-level ground-relative wind speeds in the ELDORA data within the tornado signature reached 60 m s^{-1} (Fig. 3), which is within the range that Fujita (1981) associated with F2 damage (50–69 m s^{-1}).

A significant vorticity maximum at cloud base was already present during the first Electra flight leg (2236) near the McLean storm (Fig. 3). The resolved low-level vorticity maximum was slightly weaker during the next pass, but it subsequently strengthened during the following three passes. A vorticity maximum, initially near 4 km AGL, appeared to lower and strengthen until 2259, when the magnitude of vorticity peaked at low levels. Radar observations of tornadoes in supercell thunderstorms often reveal a descending gate-to-gate tornadic vortex signature (TVS) prior to tornadogenesis (Brown et al. 1978; Trapp et al. 1999). Since the horizontal spacing between raw ELDORA observations was irregular owing to minor perturbations in the flight heading, an analysis of the gate-to-gate shear signature as a function of height and time could be misleading. However, the signature in the analysis of vertical vorticity on a broader scale (Fig. 3) is reminiscent of a descending TVS. (The complicating feature in this example is the local maximum in vorticity at low levels at 2236 prior to the descent of the vorticity maximum aloft.) The phase relationship between the vertical velocity and vertical vorticity patterns is consistent with that in Wicker and Wilhelmson's (1995) numerical simulation of the formation of a tornado-like vortex in a supercell thunderstorm. A relative maximum in upward motion aloft (at 2254 in Fig. 3) preceded the formation of the maximum in low-level vorticity (at 2259).

Although a strong low-level vorticity maximum was present early on (Fig. 3), the tornado signature in the single-Doppler data (not shown) was slow to develop. The characteristic narrow velocity anomaly with cyclonic shear was first apparent in the aft scans at 2248, when low-level ground-relative wind speeds were as high as 35 m s^{-1}. A large condensation funnel formed shortly thereafter, and low-level wind speeds had increased quickly to 60 m s^{-1} by 2254 (Fig. 3).

In a vortex-relative sense, the inflow into the pretornadic storm-scale circulation at cloud base came from the east (Fig. 2a). The analysis indicates tilting of horizontal vorticity into cyclonic vertical vorticity along the eastern and northern edges of the updraft. Farther downstream along the parcel trajectories, the analysis indicates amplification of vertical vorticity by stretching near the location of the vorticity maximum. The maintenance (and, if the analysis at 2236 is representative of earlier times, the formation) of the pretornadic vorticity maximum therefore could have involved a process of tilting and stretching in inflow from the environment (Klemp and Rotunno 1983).

During the tornadic stage, inflow into the cloud-base circulation around the tornado came more from the north (Fig. 2b). There is evidence that the supply of vertical vorticity to the tornadic region was unsteady. Although the time resolution of the dataset is not sufficient to follow conclusively the evolution of vorticity centers, the analyses from 2248 to 2259 are consistent with a merging of two vorticity maxima (Fig. 4). At 2248 (Fig. 4a), there was a separate vorticity maximum 4 km northeast of the pretornadic vorticity maximum. The separation was only 2 km during the next aircraft pass (Fig. 4b). Five minutes later, after the proposed merger, there

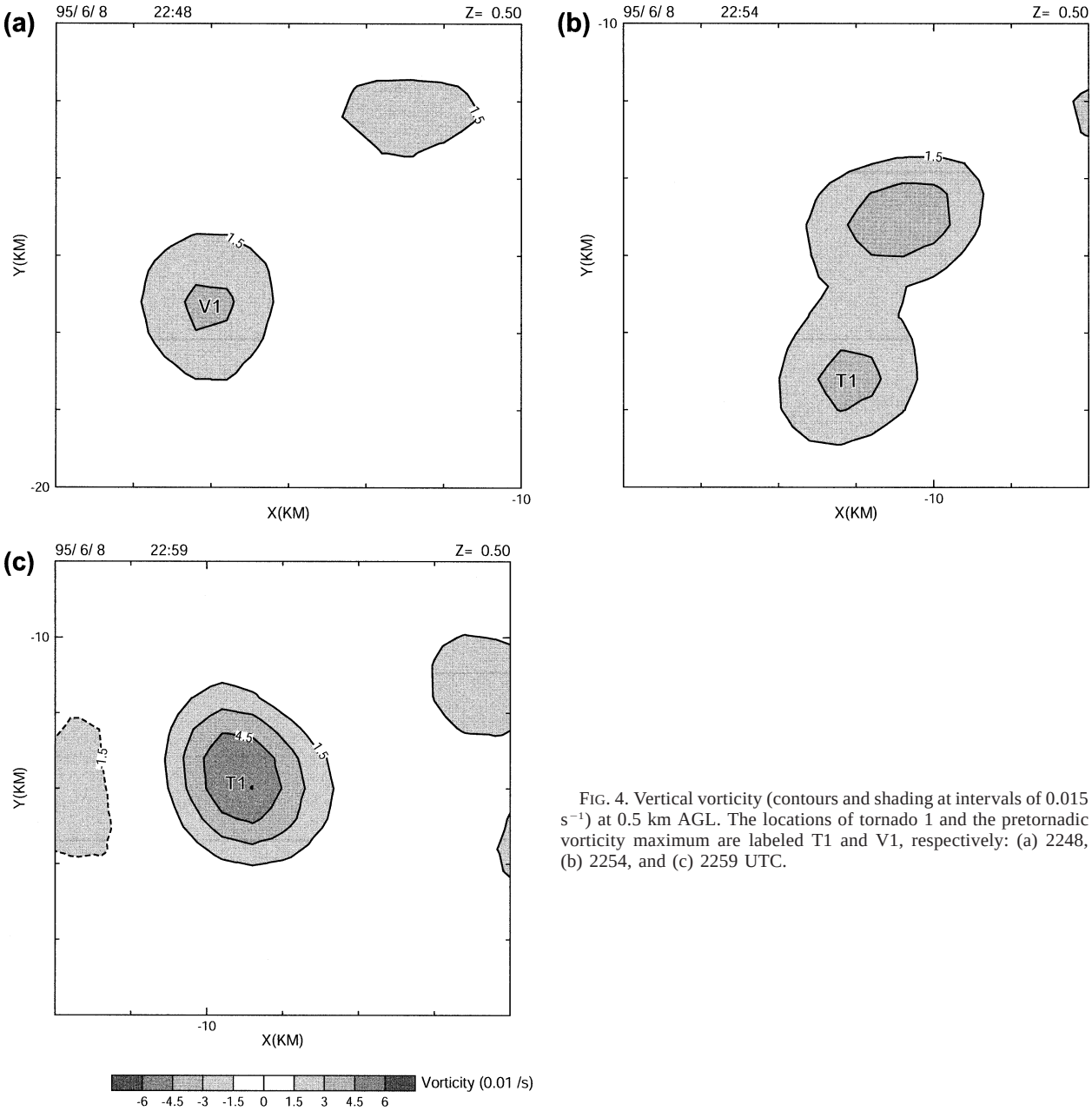

FIG. 4. Vertical vorticity (contours and shading at intervals of 0.015 s^{-1}) at 0.5 km AGL. The locations of tornado 1 and the pretornadic vorticity maximum are labeled T1 and V1, respectively: (a) 2248, (b) 2254, and (c) 2259 UTC.

was one main low-level vorticity maximum, which was more intense than either had been before (Figs. 4c and 3).

The vorticity analysis at 2254 (Fig. 2b) indicates tilting of horizontal vorticity into cyclonic vertical vorticity just northeast of, and stretching of vertical vorticity within, the secondary vorticity maximum at $x = -10.5$, $y = -12.5$ (Fig. 4b). However, there is no indication of strong stretching in the vicinity of tornado 1 itself. Presumably there was strong low-level convergence (Lewellen 1993) and thus significant stretching of vertical vorticity within the tornado. However, the region of low-level convergence was likely too shallow (Wurman et al. 1996) and too small in horizontal scale to be resolved. Centrifuging of scatterers (Dowell et al. 2001) may have also had a minor impact on the estimates of horizontal divergence and thus vertical velocity. If the dominant target producing backscattered radiation was large (1 mm) drops of rain, then the estimates of divergence in the resolved vortices may have been 0.002–0.01 s^{-1} too high. The vertical motion fields in the dual-Doppler analyses are representative of the larger-scale parent storm rather than of the tornadoes.

As tornado 1 began to weaken, its separation from the main updraft increased substantially. By 2313, the tornado was within a trailing updraft, 7 km southwest

of the center of the main storm updraft (Fig. 2c). Despite the collocation of the tornado with a broader-scale updraft, measured wind speeds in the tornado (bottom of Fig. 3), and the magnitude of vorticity in the surrounding flow at low levels (shading in Fig. 3), decreased significantly from 2259 to 2313. Because there were no measurements of winds and temperature near the surface, it is difficult to determine the exact reasons for dissipation. Since the environment was potentially very unstable (thermodynamically) for this case (Fig. 6 in Part I), a lack of surface-based CAPE in the tornado inflow does not appear to be a plausible explanation for tornado dissipation. Low-level air would have had to have been much cooler and/or drier than what was observed late in the lifetime of the storm (e.g., Fig. 1) to have lost the potential for buoyancy aloft.

Instead, we speculate that the tornado dissipated because the magnitude of low-level circulation surrounding the tornado decreased. At 2313, the flow from the north into the vorticity maximum associated with tornado 1 came from a region of relatively weak horizontal vorticity, weak tilting of horizontal vorticity into the vertical, and weak stretching of vertical vorticity (Fig. 2c). If the tornado relied on low-level circulation from the surroundings at radii of 1 km or more for sustenance, then its supply of circulation had decreased dramatically by 2313 (Fig. 3). As tornado 1 weakened, the width of both the velocity signature in the ELDORA data and the visible condensation funnel gradually decreased. The narrowing of the tornado is consistent with a decrease in swirl ratio (i.e., weaker circulation but continued strong updraft) (Ward 1972; Davies-Jones 1973).

d. The life cycle of the second storm-scale circulation

The reader is referred to Figs. 5, 6, and 7 in the following discussion. The condensation funnel of the second tornado in the McLean storm formed at 2310 and dissipated around 2322. The ground-relative wind speed in the ELDORA data at 500 m AGL was as high as 52 m s^{-1} in tornado 2 (Fig. 5). If the winds were also as strong near the surface, then the peak wind speed would be consistent with the damage rating (Fujita 1981) of F2 (NCDC 1995).

Since the radar was relatively far (~15 km) from tornado 2, the low-level horizontal vorticity field is not as well resolved as in the scans of tornadoes 1 and 4 from closer range. Nevertheless, the analyses consistently indicate tilting of horizontal vorticity into cyclonic vertical vorticity along the eastern edge of the main updraft, where a significant component of the horizontal vorticity was parallel to the vertical-velocity gradient (Fig. 6). The pretornadic low-level vorticity maximum formed along the east side of the curved main updraft, just downstream of a region of tilting (Fig. 6a).

The location of the low-level vorticity maximum had shifted more to the west side of the main updraft by the time of the ELDORA scan at 2306 (Fig. 6b). Tilting of

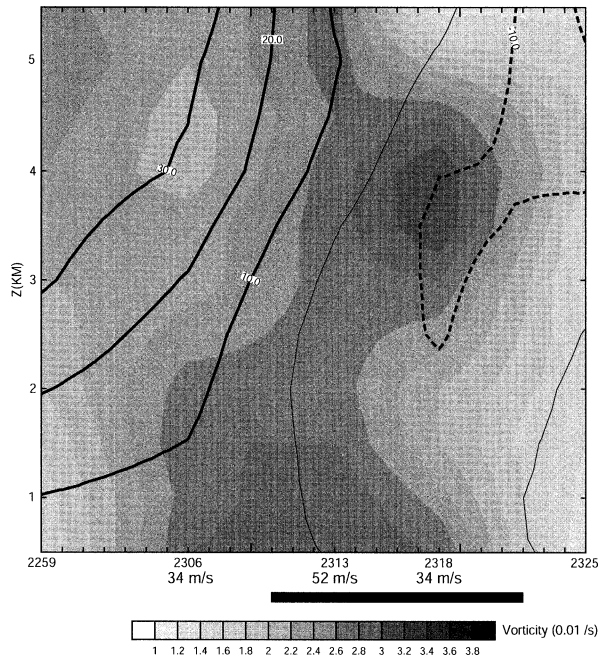

FIG. 5. As in Fig. 3 except for the vorticity maximum associated with tornado 2.

horizontal vorticity into the vertical along the eastern side of the updraft maximum, followed by stretching of vertical vorticity within the updraft core, continued to occur along inflowing trajectories from the southeast (Figs. 6a and 6b). Low-level vorticity was increasing significantly at this time (Fig. 5).

Tornado 2 formed to the west of the storm-scale vertical velocity maximum (Figs. 7a and 6c). As was the case with the previous tornado, tornado 2 became more separated from the main updraft (and the associated regions of tilting and stretching) during the mature and weakening stages (Fig. 6c). Unlike tornado 1, which dissipated in a region of updraft, the weakening tornado 2 was in a region of mean downward motion at 2318 (Fig. 5). As the tornado moved into a region of heavier precipitation to the west of the updraft (Fig. 9f in Part I), the low-level inflow may have become too dense (cool and/or precipitation loaded) to be lifted to its level of free convection (LFC). The velocity signature in the single-Doppler scans weakened but did not become narrow like that of tornado 1 (not shown). Since tornado 2 was obscured by precipitation after 2318, we cannot relate the radar signature to visual characteristics of the tornado during dissipation.

Vorticity in the resolved storm-scale circulation associated with tornado 2 increased in magnitude with height 10 min before the formation of the condensation funnel (2259 in Fig. 5) but decreased in magnitude with height shortly thereafter following the strengthening of the low-level vorticity maximum (2306 in Fig. 5). The relevance of the vorticity maximum aloft during the weakening stages of both tornadoes 1 and 2 (5 km AGL

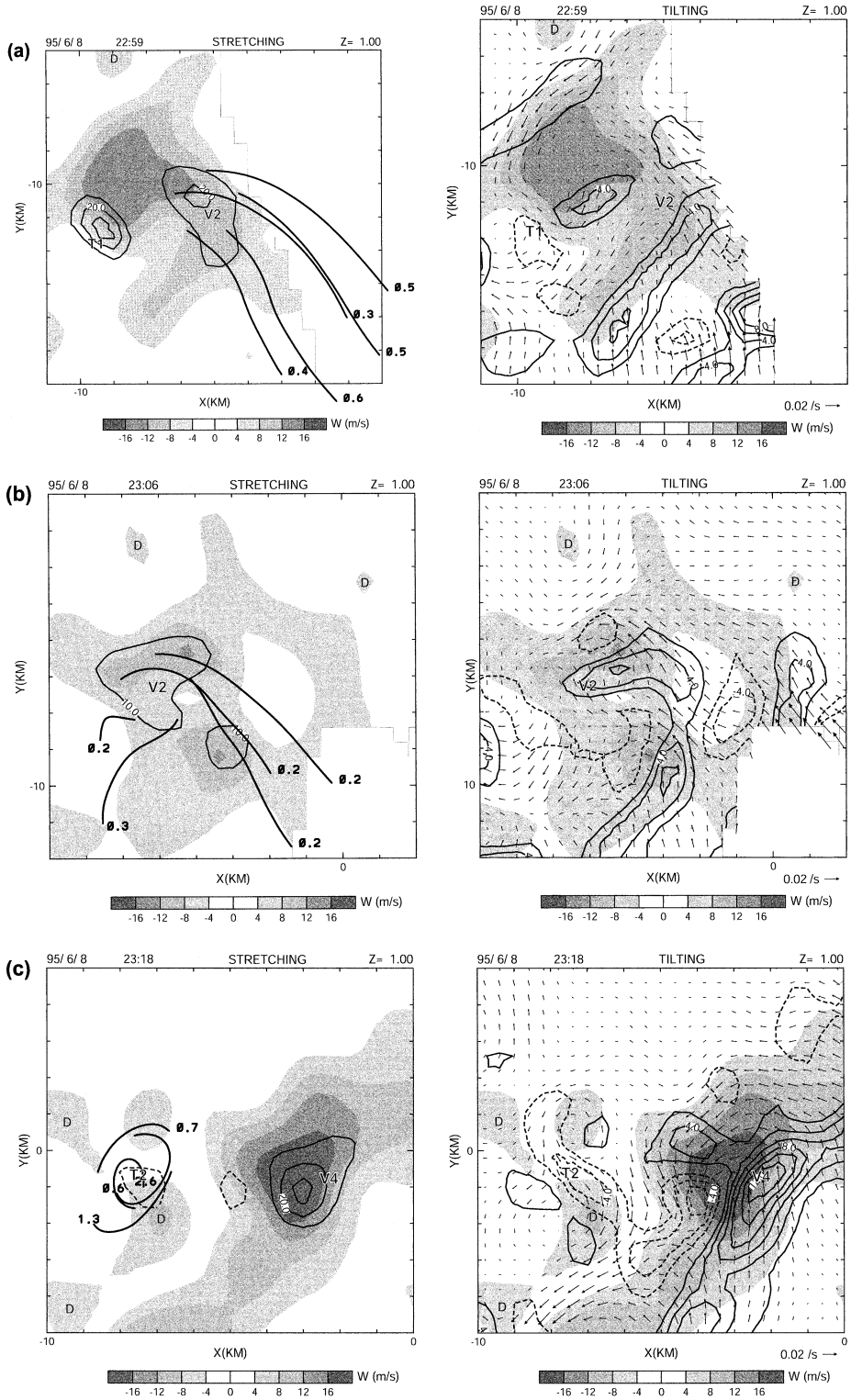

FIG. 6. As in Fig. 2 except for the life cycle of tornado 2. Tornado locations (Ts) and pretornadic vorticity maximum locations (Vs) are indicated: (a) stretching and tilting (1.0 km AGL) at 2259 UTC, (b) stretching and tilting (1.0 km AGL) at 2306 UTC, and (c) stretching and tilting (1.0 km AGL) at 2318 UTC.

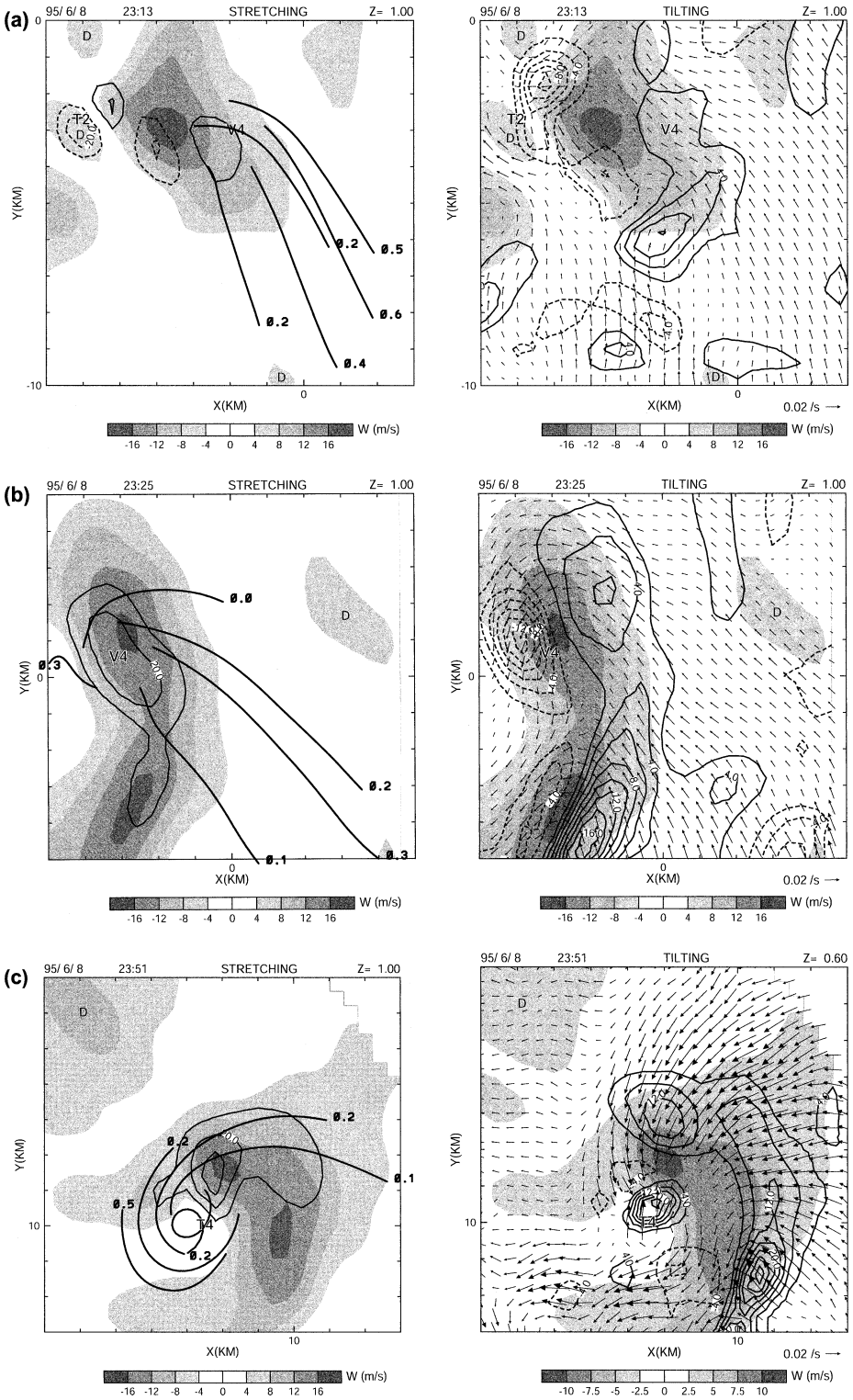
(a)
95/ 6/ 8 23:13 STRETCHING Z= 1.00
95/ 6/ 8 23:13 TILTING Z= 1.00
(b)
95/ 6/ 8 23:25 STRETCHING Z= 1.00
95/ 6/ 8 23:25 TILTING Z= 1.00
(c)
95/ 6/ 8 23:51 STRETCHING Z= 1.00
95/ 6/ 8 23:51 TILTING Z= 0.60
Y(KM)
X(KM)
0.02 /s
W (m/s)
-16 -12 -8 -4 0 4 8 12 16
-10 -7.5 -5 -2.5 0 2.5 5 7.5 10
D
T2
V4
T4

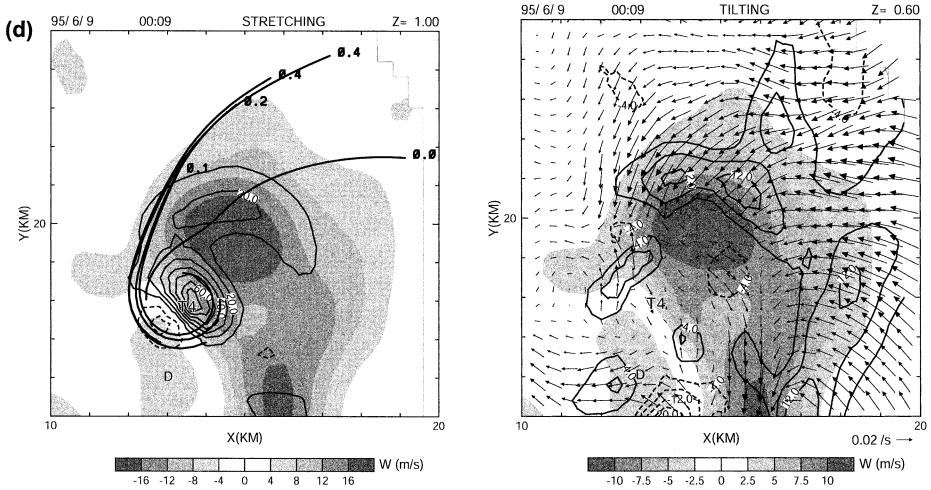

FIG. 7. As in Fig. 2 except for tornado 4: (a) stretching and tilting (1.0 km AGL) at 2313 UTC, (b) stretching and tilting (1.0 km AGL) at 2325 UTC, (c) stretching and tilting (0.6 km AGL) at 2351 UTC, and (d) stretching and tilting (0.6 km AGL) at 0009 UTC.

at 2306 in Fig. 3; 4 km AGL at 2318 in Fig. 5) is unknown. In earlier multiple-Doppler observations of tornadic storms, rotation typically decreased with height instead during the weakening stage of the tornado (Brandes 1978; Brandes 1984; Dowell and Bluestein 1997). With observations separated by 5–7 min, we find it difficult to trace the evolution of the vertical distribution of vorticity in the McLean storm. It would be tempting to explain the vorticity maximum aloft at 2306 in tornado 1 as vertical advection of the strong vorticity maximum observed at low levels at the previous time (Fig. 3). However, the situation appears to be more complicated in the case of tornado 2, in which there are simultaneous vorticity maxima near the surface and aloft (2318 in Fig. 5). We await future observations of cyclic storms with better temporal sampling to determine whether the vorticity maximum aloft is typical of cyclic storms and, if so, to see how it evolves.

e. The life cycle of the third storm-scale circulation

The reader is referred to Figs. 7, 8, 9, 10, and 11 in the following discussion. Tornado 4 in the McLean storm became visible at 2328 and persisted for at least 70 min. The tornado was still in progress when the Electra mission ended at 0015. The F4[1] damage rating of tornado 4 was higher than that of any of the other tornadoes in the McLean storm (NCDC 1995). The ELDORA data indicate wind speeds as high as 92 m s^{-1} within 1 km of the surface (Fig. 8). The peak wind speed is just below the range (93–116 m s^{-1}) that Fujita (1981) associated with F4 damage. Measurements very close to the surface on spatial scales of tens of meters would be necessary to evaluate the calibration of the wind speeds to the damage scale, but such observations are not available in the ELDORA data.

The development of the pretornadic vorticity maximum at cloud base associated with tornado 4 (i.e., the third storm-scale circulation) resembles that of previous tornadoes (cf. Figs. 2a, 6a, and 7a). Production of cyclonic vertical vorticity by tilting occurred along the eastern flank of the updraft within air parcels approaching the updraft maximum from the southeast (Figs. 7a and 7b). Stretching downstream in the updraft increased the magnitude of the vertical vorticity. During the pretornadic

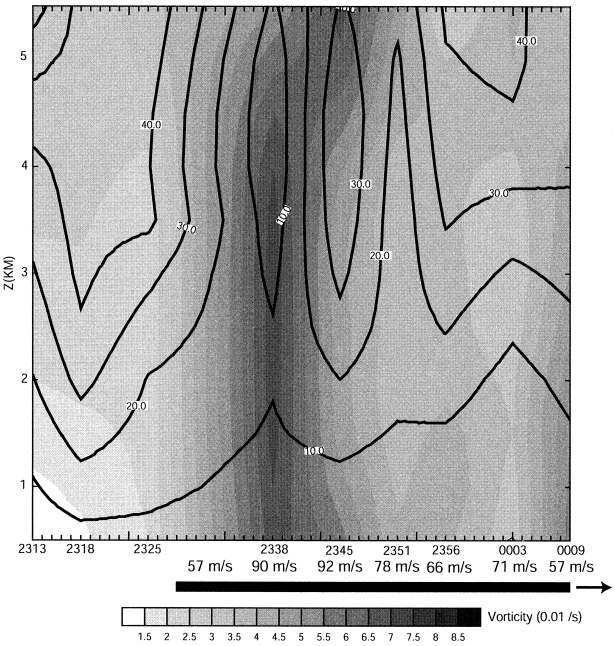

FIG. 8. As in Fig. 3 except for the vorticity maximum associated with tornado 4.

[1] R. Wakimoto (1995, personal communication), based on an exhaustive ground and aerial survey, rated the damage of tornado 4 as F5.

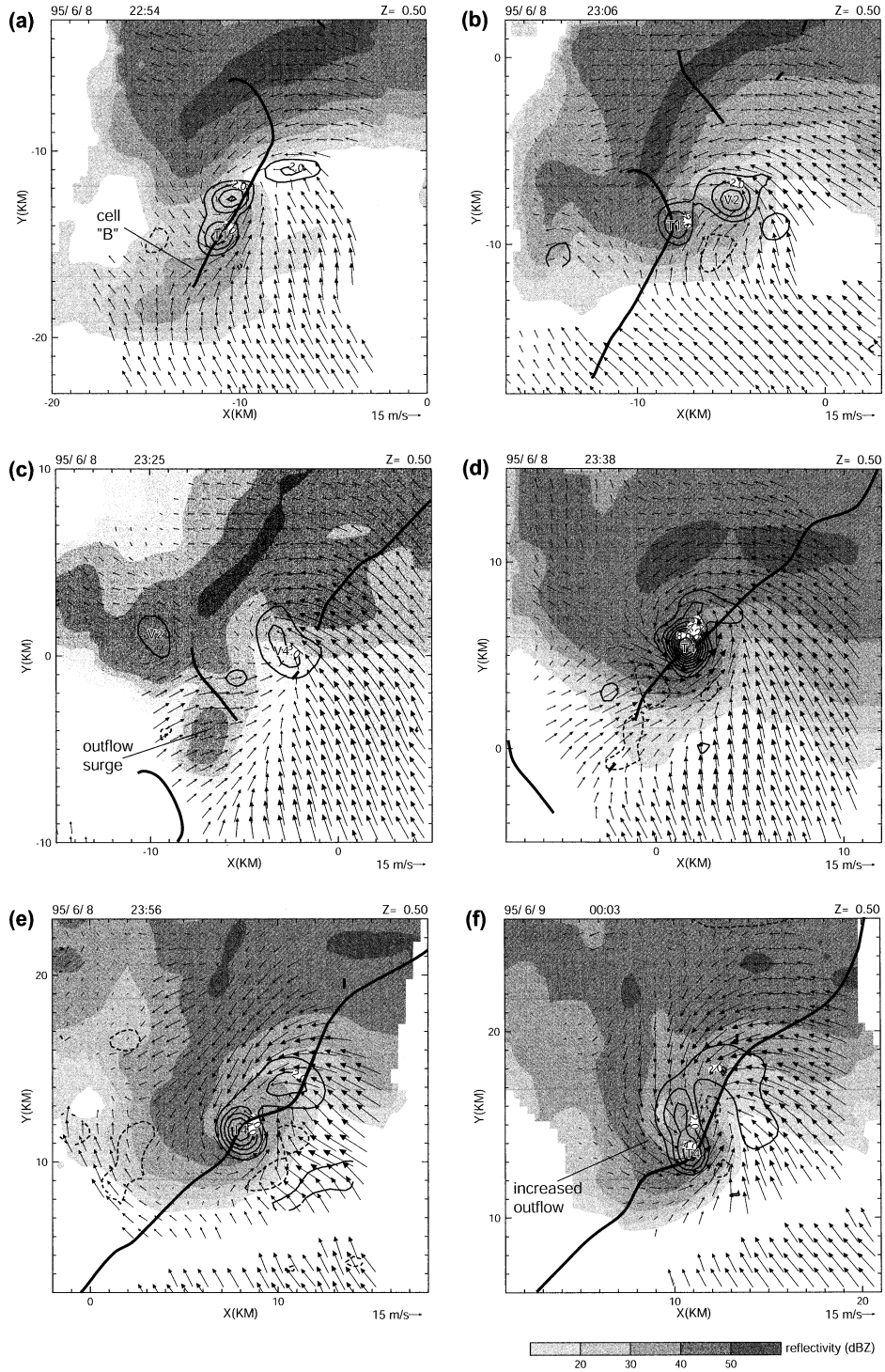

FIG. 9. Ground-relative horizontal wind (vectors, every other vector plotted), vertical vorticity (contours at intervals of 0.01 s^{-1}), and reflectivity factor (shading) at 0.5 km. Tornado paths are marked with heavy black lines: (a) 2254, (b) 2306, (c) 2325, (d) 2338, (e) 2356, and (f) 0003 UTC.

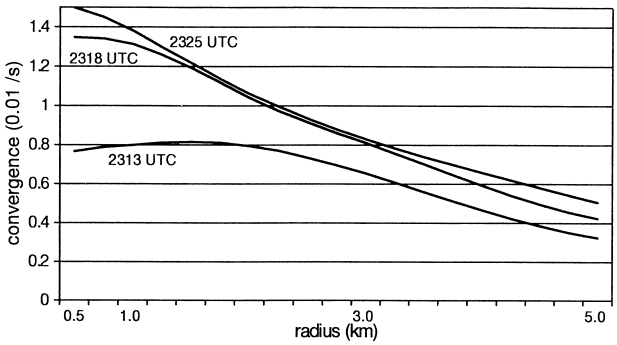

FIG. 10. Mean convergence (units of 0.01 s^{-1}) within circles of varying radii (km) centered around vortex 4 at 0.5 km AGL.

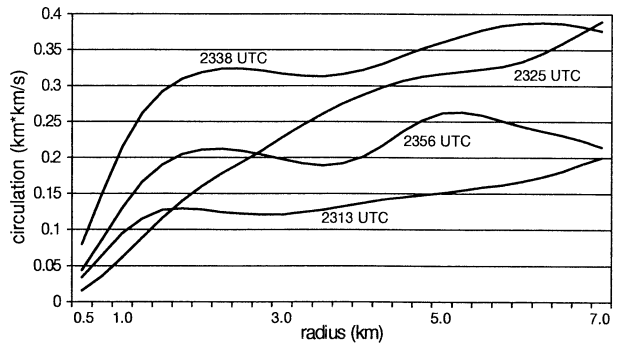

FIG. 11. Circulation ($km^2\ s^{-1}$) in a horizontal plane at 0.5 km AGL as a function of radius (km) from the vorticity maxima (vortex 2 at 2313 UTC, vortex 4 at other times).

stage, vertical vorticity in the storm-scale circulation increased with height (2313 and 2318 in Fig. 8).

At 2313, the vorticity maximum was near the eastern edge of the low-level updraft, but by 2325 it was just west of the axis of maximum upward motion (cf. Figs. 7a and 7b). In both cases, the vorticity maximum was downstream of a region where the vertical-velocity gradient at 1 km AGL was oriented approximately from east to west along the eastern side of the updraft. In section 2b, we noted that the orientation of the low-level horizontal vorticity veered with height. Therefore, there may have been a local maximum in tilting upstream of the vorticity maximum at some level below 1 km, where the orientation of the horizontal vorticity was more parallel to the vertical-velocity gradient (i.e., directed toward the west) along the eastern flank of the updraft. The analyses of tilting at 1 km do indicate positive tilting where the trajectories intersect the eastern flank of the updraft, but analyses below 1 km, were they available, could indicate a stronger relationship between the maximum in tilting and the location of the vorticity maximum.

The storm-scale circulation associated with tornado 4 became tornadic when it was southwest of the center of the maximum updraft (e.g., Figs. 7c and 7d). Trajectories approaching the mature circulation from the north pass through a region where horizontal vorticity was tilted into the vertical to the north of the updraft maximum. The orientation of the horizontal vorticity there at 600 m AGL was toward the southwest; in contrast, the horizontal vorticity in the environment to the east of the updraft was oriented toward the northwest. Downstream of the region of the tilting, the trajectories pass through the western side of the region of maximum stretching of vertical vorticity.

At 0017 and later times, the mobile mesonet identified relatively cool air northeast of tornado 4 (Fig. 1). Virtual potential temperature was 3 K higher (not shown) 20 km to the east of this location. A low-level parcel that was initially 20 km east of the updraft would have reached the updraft in roughly 2000 s as it approached the updraft from the east at approximately 10 m s^{-1} in a storm-relative sense. Although the temperature gradient was weak, the effect of baroclinity still may have been significant because the parcel residence times in the weak baroclinic zone were long. Our calculations (not shown) of the change in horizontal vorticity by baroclinic generation (Klemp and Rotunno 1983) suggest a modification $\sim$0.01 s^{-1} ($5 \times 10^{-6}\ s^{-2}$ over 2000 s). Since parcels encountered a west-to-east-directed temperature gradient to the northeast and east of the tornado, baroclinic generation could account for some of the northerly component of horizontal vorticity there. Precipitation loading may have also contributed to the rate of baroclinic generation. In general, there was a sharp reflectivity gradient along the forward flank of the storm (Fig. 9). The orientation of the horizontal vorticity at 600 m AGL (Figs. 7c and 7d) was similar to that of the contours of reflectivity—east to west on the south edge of the downshear core, and northeast to southwest where the core began to curve around the north and west sides of the updraft. In terms of water loading, the reflectivity factor measurements of up to 55 dBZ may have been equivalent to temperature (buoyancy) perturbations of ~ -1 K (Wakimoto and Cai 2000).

The strength (in terms of resolvable wind speed and vorticity) of tornado 4 around 2338 was significantly greater than that of any of the tornadoes at other times (cf. Figs. 3, 5, and 8). We note that the tornado formed around the time that a significant surge of outflow from the southwest side of the storm reached the area where the new vortex was forming (Figs. 9c and 9d). Here, we are referring to an outflow feature of $\sim$10 km in horizontal extent that originated away from tornado, rather than the smaller outflow surges and bulges in the gust front that developed near the tornadoes. We were unable to identify the origin of the outflow surge at the edge of the radar data coverage but hypothesize that its formation was at least partly related to evaporation of precipitation from the new trailing precipitation cores (Figs. 5f and 5g in Part I).

The unusual strength of tornado 4 may have been related to the outflow surge in at least two ways. First of all, horizontal convergence in the pretornadic region was increasing as the outflow surge approached (Fig.

10). Second, rotation on a broad scale (Burgess et al. 1982) about the vortex was greater during the outflow surge than it had been around previous tornadoes and around tornado 4 later on (Fig. 11). The circulation (in a horizontal plane) first increased for large radii (2325 in Fig. 11) around the developing vortex 4. Then, circulation also increased in the immediate surroundings of tornado 4 (2338 in Fig. 11). Since the outflow surge and the increase in storm-scale low-level rotation happened at the same time, the mechanism that produced the outflow surge may have also increased the low-level circulation.

f. Summary

The analyses of the McLean storm (especially the analyses in Figs. 2a, 7c, and 7d of data obtained during close aircraft passes) reveal the following common features: horizontal vorticity at approximately 500 m AGL oriented toward the northwest to the east of the updraft, and horizontal vorticity oriented toward the southwest to the north and northeast of the updraft. We consider the horizontal vorticity field to the east of the updraft to be representative of the nearby ''environment'' of the storm. However, horizontal vorticity in the near-storm environment could have been enhanced by mesoscale baroclinity (Markowski et al. 1998) and by accelerating storm inflow (Brooks et al. 1993). To the north and northeast of the updraft, the north–south component of the horizontal vorticity may have been altered within a baroclinic zone in and near the precipitation region. The presence of relatively cool air to the northeast of tornado 4 (Fig. 1) supports this hypothesis; unfortunately, measurements of low-level temperature are not available near the earlier tornadoes. The change in the orientation of the low-level horizontal vorticity between locations east and north of the updraft was gradual relative to what is typically depicted in numerical simulations of supercells (Rotunno and Klemp 1985; Adlerman et al. 1999) and in conceptual models of supercells derived from the simulations (e.g., Klemp 1987). In the simulations, relatively sharp horizontal contrasts in the horizontal vorticity field developed in regions along the forward flank with temperature gradients of $\sim$1 K km^{-1}. The weaker temperature gradients in the McLean storm (Fig. 1) would have been associated with slower rates of baroclinic modification of horizontal vorticity and, all else being equal, weaker horizontal gradients of horizontal vorticity.

Before VORTEX, the 20 May 1977 Fort Cobb, Oklahoma, case (Johnson et al. 1987) was perhaps the best multiple-Doppler documentation of a supercell that produced a family of tornadoes. We can infer a few similarities about the characteristics of the low-level horizontal vorticity field in the Fort Cobb storm to those in the McLean storm. The environmental hodograph in both cases was L shaped in the lowest few kilometers (Fig. 2b of Johnson et al. 1987; Fig. 6b in Part I). In each case, strong speed shear in the lowest 1 km was associated with significant streamwise environmental horizontal vorticity. Although the radars were apparently too far ($\sim$100 km) away from the Fort Cobb storm to resolve the environmental vertical shear within the lowest 1 km to the east and southeast of the updraft, the dual-Doppler analyses do indicate a region of enhanced low-level horizontal vorticity to the northeast of the updraft (Fig. 18 of Johnson et al. 1987), as in this case (Figs. 2a, 7c, and 7d).

The following observations are consistent with the hypothesis that a significant portion of the angular momentum in the three large tornadoes in the McLean storm came from rotation produced initially by processes on scales of 2 km or more: tornadoes 1, 2, and 4 were associated with vorticity maxima in the dual-Doppler analyses, the formation of these vorticity maxima preceded the formation of the tornadoes by over 10 min, and the vorticity maxima formed within regions where the dual-Doppler analyses indicated stretching of vertical vorticity downstream of tilting of horizontal vorticity into the vertical. Interaction of the updraft with horizontal vorticity from the nearby environment appears to explain the early development of the storm-scale circulations at cloud base associated with tornadoes 1, 2, and 4. In each case, the pretornadic vorticity maximum first appeared downstream of a region where environmental horizontal vorticity in the lowest 1 km was tilted into the vertical along the eastern flank of the main updraft (Figs. 2a, 6a, and 7a). The increase in vertical vorticity with height from low to midlevels approximately 10 min before the appearance of each condensation funnel (2242 in Fig. 3, 2259 in Fig. 5, 2318 in Fig. 8) is consistent with theoretical models of tilting of approximately streamwise horizontal vorticity into the vertical, followed by horizontal advection, stretching, and vertical advection of vertical vorticity in rising air (Davies-Jones and Brooks 1993; Walko 1993).

The orientation of the horizontal vorticity below 1 km AGL varied about the updraft such that there was tilting of horizontal vorticity into cyclonic vertical vorticity along both the eastern and northern sides of the updraft (Figs. 2a, 7c, and 7d). The inflow into the vorticity maxima associated with mature tornadoes generally came from the north in a storm-relative sense (Figs. 2b, 7c, and 7d). The nature of the horizontal vorticity that fed a particular vorticity maximum changed with time as the updraft-relative position of the vortex changed. A new vertical vorticity maximum on the east side of the updraft developed from horizontal vorticity that was essentially characteristic of the nearby storm environment (Figs. 6a and 7a). As the location of the vortex changed relative to the updraft, the source of rotation became the horizontal vorticity that had been locally modified by internal storm processes (e.g., Figs. 7c and 7d). The schematic in Fig. 12 (also discussed in Part I of this paper) is a summary of the low-level dynamics for the observed storm. In the schematic, we describe the horizontal vorticity northeast of the updraft

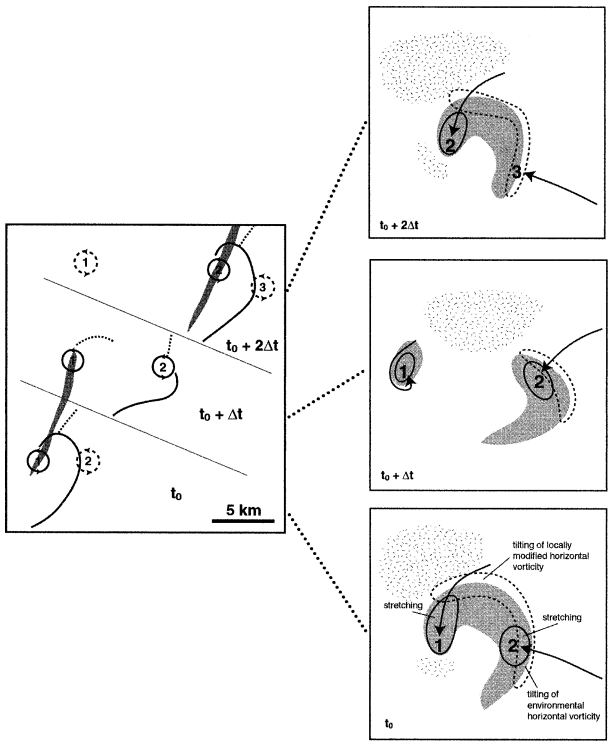

FIG. 12. Schematic at low levels of cyclic supercell tornadogenesis. (left) Numbered circles identify vortices, and the thick lines indicate wind shift lines. Tornado tracks are shaded. (right) Shading indicates updraft, and the spotted pattern indicates downdraft. Dashed (solid) outlines indicate regions of production of cyclonic vertical vorticity by tilting of horizontal vorticity (stretching of vertical vorticity). Arrows indicate vortex-relative trajectories. The time between successive tornadoes ($2\Delta t$) is ~20 min.

as ''locally modified'' to indicate the superposition of baroclinic effects onto the environmental horizontal vorticity (Wicker 1996; Dowell and Bluestein 1997). Our description of the formation of low-level rotation during the tornadic stage as a process of tilting and then stretching in air parcels moving southward through the northwestern lobe of the updraft is quite similar to the classical model by Rotunno and Klemp (1985). However, for this case, both the environment and internal storm processes appear to control the characteristics of the low-level horizontal vorticity that is converted into rotation about a vertical axis.

Davies-Jones and Brooks (1993) and Walko (1993) hypothesized that, in the absence of preexisting vertical vorticity, intense rotation near the surface cannot develop in purely rising air. Tilting in a downdraft in the Davies-Jones and Brooks (1993) simulation occurred to the north-northwest of the updraft, where the horizontal vorticity was directed toward the south-southeast. In the McLean storm, there was a region of tilting at 500–600 m AGL to the north of the updraft maximum, where the horizontal vorticity was directed toward the south-southwest (Figs. 2a, 7c, and 7d). However, the region of positive tilting in the analysis at 600 m does not extend into the downdraft region. Furthermore, the low-level downdraft region to the north and northwest of the updraft tended to be relatively weak, and in only a few analyses (e.g., Fig. 7c) is its strength greater than the magnitude corresponding to the first level of shading in the figures. An argument supporting a critical role of the downdraft in mesocyclogenesis near the surface would therefore be based only on the circumstantial evidence that low-level intensification of each vortex did not occur until the low-level trajectories approached from the north (i.e., the side of the updraft that was flanked by the downdraft). Since tilting in a downdraft in the numerical simulations (Davies-Jones and Brooks 1993) was particularly important within a few hundred meters of the surface, one could speculate that observations closer to the surface than were available from the ELDORA would have been necessary to reveal such a process.

Near a smaller, separate rear-flank downdraft ($x = -7$, $y = -2$ in Fig. 6c; $x = 13$, $y = 16$ in Fig. 7d) (Klemp and Rotunno 1983) that tended to appear to the south of mature tornadoes, there was no consistent pattern of positive tilting. We also considered the role of vertical advection of vertical vorticity (Fujita 1973, 1975; Das 1983; Davies-Jones 2000) in this portion of the downdraft. We found examples only of transport of lesser values of cyclonic vorticity downward (not shown) in the 500–1000-m layer. If this downdraft played a direct role in the vorticity dynamics of low-level mesocyclogenesis, then its importance also must have been greatest below the lowest level of observations.

3. Cyclic tornado formation

We postulate that a long-lived tornado persists in a region where the air near the surface is rich in vertical vorticity, is convergent, and is potentially buoyant. In a cyclic storm, conditions must be only periodically conducive to tornado formation and maintenance, or the tornadoes that do form must not remain in that portion of the storm where conditions are favorable for maintenance. Since the McLean storm produced tornadoes almost continuously over nearly 2 h, we suggest that the latter was true during the cyclic stage. Burgess et al. (1982) suggested that successive tornadoes in cyclic storms form primarily via stretching of ambient low-level vertical vorticity. However, the analyses of the McLean storm indicate a strong association between tilting of horizontal vorticity into the vertical and new vortex formation, as noted in Adlerman et al.'s (1999) numerical simulation experiments.

A qualitative description of cyclic tornadogenesis in the McLean storm was provided in Part I of this paper. The evolution resembles that in previous conceptual models of cyclic storms (Burgess et al. 1982; Klemp 1987; Adlerman et al. 1999) in terms of the location in which new vortices formed with respect to the rear-flank gust front (Fig. 12). However, successive tornadoes did not appear to be associated with discrete propagation of

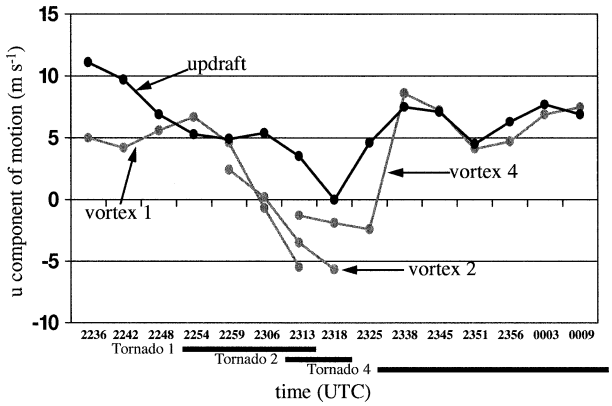

FIG. 13. Eastward component of motion (m s^{-1}) as a function of time of the updraft and the three main vorticity maxima. The motions are from finite-difference approximations based on consecutive locations of the vorticity maxima at 0.5 km AGL and the centers of the updraft at 4 km AGL. The bars at the bottom of the figure indicate the time periods when tornadoes were observed.

TABLE 1. Typical magnitude (maximum values $\times$ 10^{-5} s^{-2} at a grid point in/near the tornadic vortices), as a function of height, of terms in the frictionless vertical vorticity equation, for the dual-Doppler analyses of the McLean storm. In the first term (horizontal advection), the values of u and v are relative to the motion of the updraft.

Term in vorticity equation	Height (km AGL)			
	0.5	1.0	3.0	5.0
$\left\lvert -\left(u\frac{\partial}{\partial x} + v\frac{\partial}{\partial y}\right)\zeta \right\rvert$	30	30	30	40
$\left\lvert -w\frac{\partial \zeta}{\partial z} \right\rvert$	10	20	40	40
$\left\lvert \frac{\partial u}{\partial z}\frac{\partial w}{\partial y} - \frac{\partial v}{\partial z}\frac{\partial w}{\partial x} \right\rvert$	5	10	25	20
$\left\lvert -\left(\frac{\partial u}{\partial x} + \frac{\partial v}{\partial y}\right)\zeta \right\rvert$	40	30	20	20

the main storm updraft as in previous conceptual models. Instead, the tornadoes formed near, and occasionally became separated from, a single persistent main updraft.

The focus in this section is primarily on a discussion of the following questions: Why did the storm produce a family of tornadoes rather than only one tornado? Why was the fourth tornado longer lived than the other tornadoes? The key element in the traditional description of the cyclic process is the outflow along the rear flank of the storm. During the tornadic stage, outflow from the rear-flank downdraft may surround the vortex and undercut the updraft, cutting off the supply of potentially buoyant air (Lemon and Doswell 1979; Burgess et al. 1982; Klemp 1987; Brooks et al. 1994; Adlerman et al. 1999). Although the outflow may be destructive to the original updraft and tornado, the leading edge of the outflow may initiate new updraft growth and vortex formation nearby.

For the high-CAPE environment of the McLean storm, it is unlikely that the tornadoes dissipated because they were cut off from potentially buoyant low-level air (discussed previously in section 2c). Tornado 1 was within updraft when it dissipated (Figs. 2c and 3). However, there had been a significant decrease in the magnitude of low-level circulation in the surrounding flow within a radius of 1 km (Fig. 3). In contrast, tornado 2 dissipated within a region of mean downward motion (Fig. 5). Although potentially buoyant, the low-level air apparently was not being lifted to its LFC. Both tornadoes dissipated when they became separated from the main updraft.

The mean motion of the updraft in the McLean storm during the period of survey by the ELDORA was to the northeast at 9.5 m s^{-1}. Although the motion was not constant, it was less variable than the motions of individual tornadoes (Fig. 13). In Fig. 13, we focus on the u component of motion since it tended to vary more than the v component. The first two vorticity maxima and tornadoes did not keep up with the eastward motion of the main updraft. The typical life cycle of a storm-scale circulation involved formation along the east side of the updraft, maturation near the northwest lobe of the updraft, and weakening as it was shed rearward (Fig. 12).

From the frictionless form of the vertical vorticity equation, we expect the location of a local maximum in vorticity to change whenever the forcing (sum of horizontal advection of vertical vorticity, vertical advection of vertical vorticity, tilting of horizontal vorticity into the vertical, and stretching of vertical vorticity) is out of phase with the vortex. As a crude estimate of the magnitude of the forcing terms in the vorticity equation for this case, we identified typical maximum values based on the wind syntheses (Table 1). In the calculations of horizontal advection, the horizontal wind components relative to the motion of the updraft are used. We estimated the horizontal velocity of the updraft at each time from the locations of the center of the updraft at 4.0 km (a level at which the main updraft tended to be circular) at the most recent and next analysis times.

Since stretching and horizontal advection are the dominant terms at the lowest levels (Table 1), a low-level vortex will tend to move toward local maxima in these quantities. Although the magnitude of tilting is relatively small at low levels, the vortices are, in the absence of ambient vertical vorticity, constrained to form downstream of the weak but broad regions of tilting. Aloft, the magnitudes of the terms in the vorticity equation are more comparable. For the resolution of the Doppler syntheses, the values in Table 1 apply to horizontal scales of greater than 2 km. On the scale of the tornado itself, we are especially interested in very low levels since this is the location of the maxima in wind speed and vorticity (Fiedler 1993; Lewellen 1993).

The relative importance of horizontal advection at low levels (Table 1) indicates that a tornado's motion could

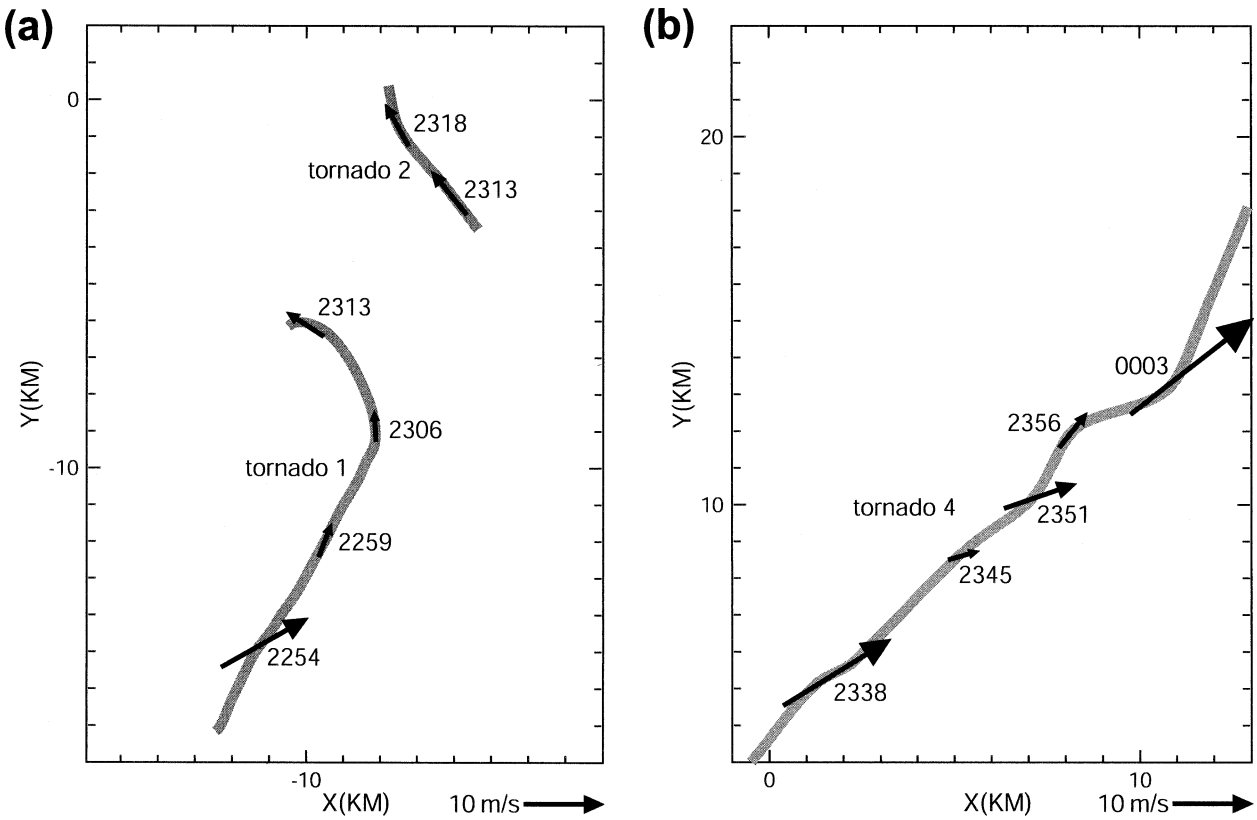

FIG. 14. Tornado tracks (gray lines) and mean ground-relative horizontal winds at 500 m AGL (vectors) in the vicinity of the tornadoes. The mean winds were computed within circles of diameter 4 km centered on the tornadoes: (a) tornadoes 1 and 2 and (b) tornado 4.

be strongly related to the mean flow in which it is embedded. To test this idea, we computed the mean horizontal wind in the vicinity of each tornado at the lowest grid level at each analysis time (Fig. 14). We calculated the mean wind over a circle that was 4 km wide and centered on the tornado. We chose a radius large enough to contain the regions of vertical vorticity greater than 0.01 s^{-1}. The mean values do depend on the choice of the diameter, but the qualitative results are insensitive to this choice. The relationship between the mean wind and the direction of tornado motion (Fig. 14) is striking, especially when one considers that the computations were for one level only, rather than for a layer.

A number of different storm-scale surges of outflow in the McLean storm modified the low-level flow in the tornadic region. The initial motion of tornado 1 was similar to the mean horizontal wind at 500 m in the tornadic region, that is, from southwest to northeast (Fig. 14a). With time, the outflow perturbation at the rear of the storm weakened, and the flow became more dominated by easterly inflow from the environment (Figs. 9a and 9b). (For example, the winds to the west and northwest of tornado 1 were more easterly than before.) In response, tornado 1 turned to the northwest (2313 in Fig. 14a). In the same time period, the north-northwesterly motion of the new vortex 2 was also to the left of the overall storm track, which was toward the northeast. When the surrounding flow later veered slightly (2318 in Fig. 14a), tornado 2 turned more to the north (i.e., to the right).

A new surge of low-level outflow began to show up within the trailing precipitation region (Fig. 5f in Part I) at 2313 (not shown). By 2325, the wind perturbation had expanded, and westerly winds dominated the southwest side of the storm (Fig. 9c). The outflow from the southwest persisted into the intense phase (2335–2350) of tornado 4 (Fig. 9d). At that time, the mean flow in the vicinity of tornado 4 was strong and from the west-southwest (Fig. 14b).

In some previous studies (e.g., Agee et al. 1976), turns in tornado tracks were attributed to rotation of the tornado about a larger vortex. This conceptual model may apply to tornado 4 at 2356 and 0003 (Figs. 9e and 9f), when the tornado was southwest and then south of the center of a region of cyclonic flow that was ~10 km wide. The enhanced westerly flow in this location relative to the broad-scale circulation may have affected the motion of tornado 4. In addition, vortex-relative motions associated with interactions of the storm-scale vorticity maxima may have been important when the earlier vortices were close (e.g., Fig. 9b). However, we are suggesting here a more important relationship be-

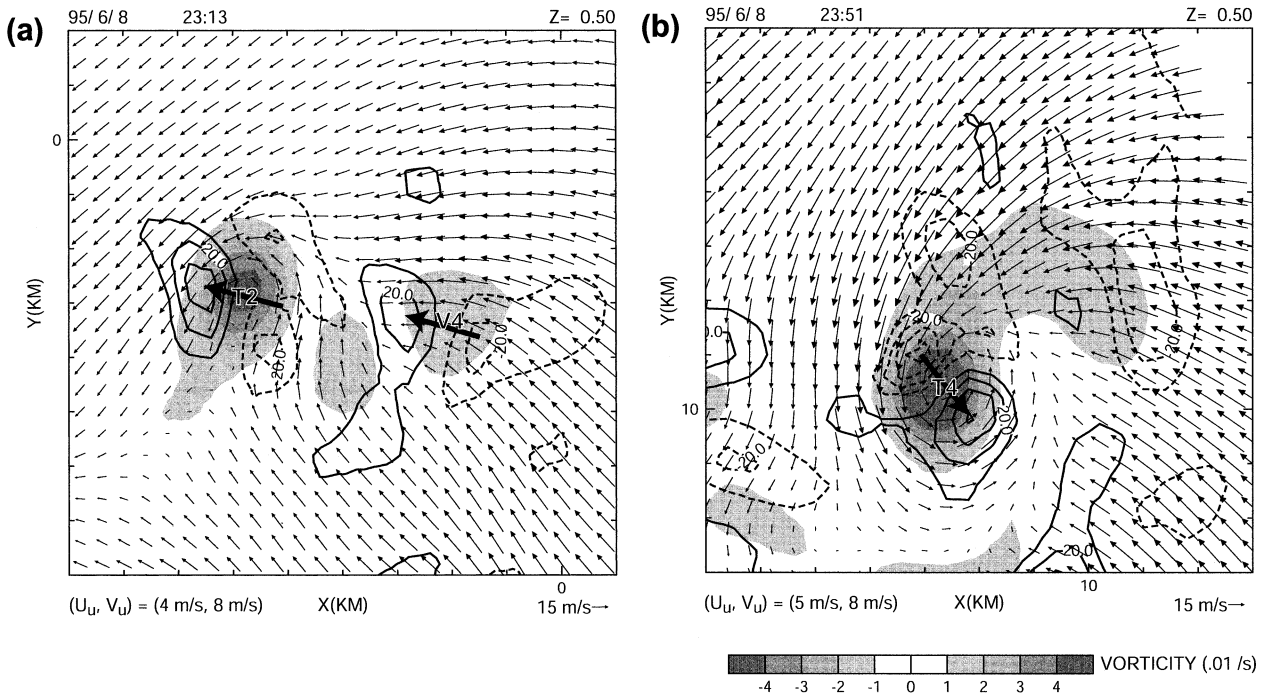

FIG. 15. Horizontal velocity (vectors), vertical vorticity (shading at intervals of 0.01 s^{-1}), and horizontal advection of vertical vorticity (contours at intervals of 10×10^{-5} s^{-2}) at 0.5 km AGL. The wind and advection patterns are given relative to the motion of the updraft (U_u and V_u, lower left). A large arrow indicates the direction a vortex would tend to move (i.e., from negative to positive values of advection of vertical vorticity): (a) 2313 and (b) 2351 UTC.

tween tornado motion and the relative strengths of the inflow and outflow winds in the tornadic region.

Viewed in the reference frame of the updraft, changes in the local mean wind around a vortex change the magnitude and/or direction of movement caused by horizontal advection (Fig. 15). When easterly updraft-relative winds penetrated deep into the storm (Fig. 15a), the pattern in the advection fields favored movement of the vortices to the west-northwest with respect to the updraft. At later times (e.g., Fig. 15b), there was more westerly momentum in the tornadic region (e.g., northerly winds now west of the tornado and westerly winds south of the tornado) despite the stronger inflow farther east. At 2351, the forcing from horizontal advection was toward the southeast (Fig. 15b), that is, toward the updraft at the gust-front bulge (Fig. 7c) rather than away from it.

Unlike the previous tornadoes, tornado 4 did not lag well behind the main updraft while the ELDORA was scanning the storm (Fig. 13). Based on the model in this section, we attribute this partly to a balance between storm-relative outflow and inflow that, on average, yielded relatively weak mean updraft-relative low-level flow in the tornadic region. This balance allowed the tornado to remain in a location where it could take advantage of a continuous supply of vertical vorticity in trajectories from the north (Figs. 7c and 7d). However, tornado 4 was still subject to changes in the forcing from horizontal advection. For example, at 2356, the mean ground-relative wind around the tornado backed, and the tornado turned slightly to the left (Fig. 14b). Within only 7 min, a new surge of outflow had developed, as indicated by a change in the direction of the winds within the reflectivity appendage from north-northeasterly to north-northwesterly (Figs. 9e and 9f); the winds in the vicinity of the tornado were once again strong from the west-southwest (Fig. 14b). Had the new outflow surge not developed around 0003, we speculate that renewed cyclic behavior may have occurred, because tornado 4 would have moved westward relative to the updraft.

In our discussion, we have implied that the parent storm supports a broad region in which a tornado, once formed, can be sustained while moving with respect to the center of the main updraft. Propagation of the updraft by dynamic pressure forcing could lead to a tendency for the updraft to move ahead of a smaller feature such as a tornado. For the dual-Doppler analyses of the McLean storm, dynamic pressure retrievals (Klemp and Rotunno 1983) consistently indicate a minimum in $\partial p_{\mathrm{dn}}/\partial z$ (i.e., a maximum in forcing for upward motion) centered east of the low-level updraft maximum (e.g., Figs. 16a and 16c) (Cai and Wakimoto 2001). We investigated the contributions to the total dynamic pressure from individual components, namely the fluid extension term,

$$\left\{\nabla^2 p_s = -\rho\left[\left(\frac{\partial u}{\partial x}\right)^2 + \left(\frac{\partial v}{\partial y}\right)^2 + \left(\frac{\partial w}{\partial z}\right)^2 - w^2\frac{d}{dz}\left(\frac{1}{\rho}\frac{d\rho}{dz}\right)\right]\right\};$$

the curvature term,

$$\left[\nabla^2 p_c = -2\rho\left(\frac{\partial v}{\partial x}\frac{\partial u}{\partial y}\right)\right];$$

and the shear term,

$$\left[\nabla^2 p_s = -2\rho\left(\frac{\partial u}{\partial z}\frac{\partial w}{\partial x} + \frac{\partial v}{\partial z}\frac{\partial w}{\partial y}\right)\right]$$

(Klemp and Rotunno 1983). Although some of the contribution to the forcing for upward motion came from the curvature term (not shown), more generally the local minimum in $\partial p_{\mathrm{dn}}/\partial z$ to the east of the updraft maximum was associated with the shear term (Figs. 16b and 16d). Dynamic pressure forcing consistently favored eastward propagation of the updraft.

The causes of updraft and tornado movement are not entirely independent, however. For example, we speculate that the eastward motion of the updraft temporarily decreased from 2306 to 2318 (Fig. 13) for the same reason that the tornadoes moved to the west—the mean low-level winds in the updraft and tornadic region were more easterly during this period (Fig. 9b).

4. Conclusions

As each major tornado in the McLean storm formed, air to its right advanced, producing a small-scale bulge in the gust front (Fig. 12). This gust-front bulge sharpened the vertical velocity gradient in the updraft ahead of the tornado. Localized strong tilting along the forward flank of the updraft produced a new maximum in vertical vorticity. The broad but weak new vortex quickly developed a profile of increasing rotation with height owing to the accumulated effects of tilting and stretching in rising air.

Updraft-relative horizontal advection carried the developing storm-scale circulation to the rear side of the updraft (Fig. 12). As the location of the vortex relative to the center of the updraft changed, the low-level trajectories into the vorticity maximum came more from its left (with respect to overall storm motion). The trajectories were ideal for carrying vertical vorticity, which was produced by tilting of horizontal vorticity into the vertical near the left side of the updraft, into the convergent roots of the updraft, where it was amplified by stretching. As the vortex reached tornadic intensity at low levels, a gust front (wind shift line) swept about the right side of the tornado and initiated yet further vortex development. The tornado persisted near the rear side of the main updraft if the location and strength of low-level outflow were such that there was weak updraft-relative flow in the tornadic region.

The storm-scale circulation associated with the long-lived tornado 4 was fed by vertical vorticity produced by tilting along an arc near the gust front (Figs. 7c and 7d). A strong tornado moving at approximately the same velocity as the updraft would tend to absorb local vorticity maxima that formed in the inflow from this region, as occurred at least twice in the McLean storm. During the early life of tornado 1, the vorticity maximum to its north-northeast (Fig. 4) apparently did not have time to mature before being absorbed. Much later, a narrow tornado 5 formed north-northeast of the intense tornado 4 (Fig. 4d in Part I). The remnant funnel cloud was observed visually to be drawn into tornado 4.

Cyclic tornado formation may result if the horizontal motion of the tornadoes repeatedly does not match the horizontal motion of the main storm-scale updraft and downdraft. Each tornado in the McLean storm formed near the rear part of the main updraft. Horizontal advection forced the first two tornadoes westward relative to the updraft. Both tornadoes persisted for a while as their separation from the main updraft increased to several kilometers. We speculate that each tornado eventually dissipated when its low-level inflow either lacked vorticity or was too dense to be lifted to the LFC. Westward advection of the tornadoes relative to the updraft occurred during the stage in the storm's life when low-level outflow was relatively weak, and southeasterly inflow penetrated to the back of the storm. In other storms, the mismatch of the motions of the tornadoes and the updraft may be related to discrete propagation of the updraft.

A diagnosis of the formation of low-level outflow was beyond the scope of this paper. Since the mobile mesonet did not observe cold air behind the rear-flank gust front near tornado 4, the formation of outflow may have involved more complicated processes than evaporation of precipitation alone. The strength of outflow from the rear of the storm appeared to influence both the strength of individual tornadoes and whether tornadoes were cyclic or long lived. The surge of outflow that coincided with the end of the cyclic phase (and the formation of tornado 4, the strongest tornado in the family) followed the formation of updrafts and precipitation to the southwest of the main cell. Earlier, although there was no large-scale perturbation in the flow apparent, tornado 1 also formed when precipitation from a neighboring cell interacted with the main storm (cell B in Fig. 9a and in Fig. 5b in Part I). *This type of evolution involving interaction of cells would be difficult to anticipate in advance from environmental parameters.* In some cyclic storms, transitions between nontornadic and cyclic tornadic, and between cyclic tornadic and long-lived tornadic stages may be related to other factors such as changes in the environment or the degree of maturity of the storm.

The lack of measurements near the surface in this case was a serious problem in the estimation of low-level trajectories and the evaluation of forcing in the vorticity equation. Analyses of horizontal vorticity and tilting as low as ~500 m AGL (Figs. 2a, 7c, and 7d) were possible only for ELDORA data collected within ~10 km of the target. Very close to the surface, surface drag may have played a significant role in organizing the horizontal vorticity field. The increase in wind speed

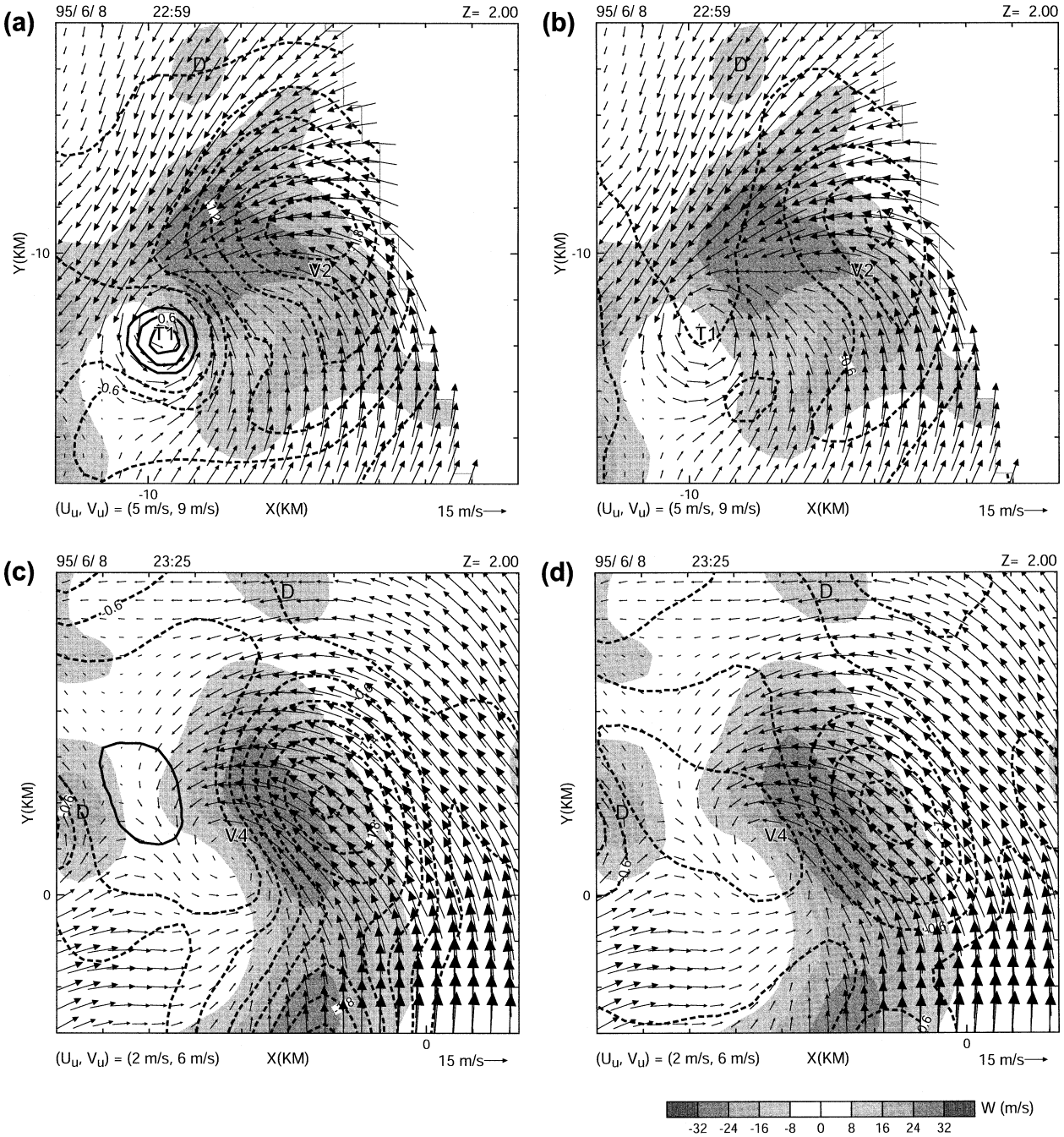

FIG. 16. Horizontal updraft-relative wind (vectors), vertical velocity (shading, downdrafts labeled with a D), and vertical derivative of dynamic pressure (contours, negative values contoured with dashed lines) at 2.0 km AGL. The contour interval is 0.3 mb km^{-1}. Plots are shown of both the total dynamic pressure gradient ($\partial p_{dn}/\partial z$) and the pressure gradient associated with the shear term ($\partial p_s/\partial z$), where $\nabla^2 p_s = -2\rho[(\partial u/\partial z)(\partial w/\partial x) + (\partial v/\partial z)(\partial w/\partial y)]$. Regions of negative (positive) $\partial p_{dn}/\partial z$ are associated with forcing for upward (downward) motion. The boundary conditions for the pressure retrieval are the same as those of Klemp and Rotunno (1983): (a) $\partial p_{dn}/\partial z$ at 2259 UTC, (b) $\partial p_s/\partial z$ at 2259 UTC, (c) $\partial p_{dn}/\partial z$ at 2325 UTC, and (d) $\partial p_s/\partial z$ at 2325 UTC.

from zero at the ground to ~20 m s^{-1} at 200 m (Fig. 6 in Part I) was associated with strong horizontal vorticity (~0.1 s^{-1}) in the surface layer. Since the direction of storm motion was approximately perpendicular to the vertical shear near the surface, there was significant streamwise horizontal vorticity in the surface layer. These characteristics of the horizontal vorticity field are neither resolved in the radar data nor are they included in standard numerical simulations with a free-slip lower boundary.

For a more definitive diagnosis of tornadogenesis from observations, in future cases we require coordinated mobile, ground-based radar (Wurman et al. 1997; Bluestein and Pazmany 2000; Biggerstaff and Guynes 2000) and in situ measurements taken from very close to the storm in order to obtain detailed information in the lowest 100 m. These measurements should be complemented by observations from radars that scan the rest of the storm aloft. To document the formation and dissipation of 1-km scale features, updates approximately every 1 min will be required.

Acknowledgments. This work was funded by National Science Foundation Grants ATM-9612674 and ATM-991209, and was completed while the lead author was supported by the Cooperative Institute for Mesoscale Meteorological Studies (NSF Grant ATM-000412). We thank all VORTEX participants for their contributions. In particular we acknowledge Erik Rasmussen for leading the field project, Roger Wakimoto for directing the Electra aircraft operations, the NOAA P-3 and NCAR Electra flight crews for making the collection of airborne Doppler data possible, and Jerry Straka for helping design and coordinate the mobile mesonet operations.

Wen-Chau Lee provided the ELDORA data and answered many questions about data processing. Michelle Case and Dick Oye assisted with the REORDER objective analysis software. The Grid2ps software by Susan Stringer and Wen-Chau Lee was an essential tool in the development of graphics for this paper. David Ewoldt, Bruce Haynie, Cristina Kaufman, Tim Marshall, Scott Richardson, and Herb Stein provided video and photographic documentation of the McLean storm. Doug Crowley supplied information on the surveys of the McLean tornadoes by the Amarillo, Texas, National Weather Service office. We appreciate the input of the following individuals on various aspects of this work: Chuck Doswell, Matt Gilmore, Mike Magsig, Morris Weisman, and Lou Wicker. In addition, the comments of three anonymous reviewers were quite helpful. This research would not have been possible without the computer assistance of Tom Condo and Mark Laufersweiler at the University of Oklahoma.

REFERENCES

Adlerman, E. J., K. K. Droegemeier, and R. Davies-Jones, 1999: A numerical simulation of cyclic mesocyclogenesis. *J. Atmos. Sci.,* **56,** 2045–2069.

Agee, E. M., J. T. Snow, and P. R. Clare, 1976: Multiple vortex features in the tornado cyclone and the occurrence of tornado families. *Mon. Wea. Rev.,* **104,** 552–563.

Barnes, S. L., 1968: On the source of thunderstorm rotation. National Severe Storms Laboratory Tech. Memo. ERLTM-NSSL 38, 28 pp. [NTIS PB-178990.]

Biggerstaff, M. I., and J. Guynes, 2000: A new tool for atmospheric research. Preprints, *20th Conf. on Severe Local Storms,* Orlando, FL, Amer. Meteor. Soc., 277–280.

Bluestein, H. B., and A. L. Pazmany, 2000: Observations of tornadoes and other convective phenomena with a mobile, 3-mm wavelength, Doppler radar: The spring 1999 field experiment. *Bull. Amer. Meteor. Soc.,* **81,** 2939–2951.

Brady, R. H., and E. J. Szoke, 1989: Case study of nonmesocyclone tornado development in northeast Colorado: Similarities to waterspout formation. *Mon. Wea. Rev.,* **117,** 843–856.

Brandes, E. A., 1978: Mesocyclone evolution and tornadogenesis: Some observations. *Mon. Wea. Rev.,* **106,** 995–1011.

——, 1981: Finestructure of the Del City–Edmond tornadic mesocirculation. *Mon. Wea. Rev.,* **109,** 635–647.

——, 1984: Vertical vorticity generation and mesocyclone sustenance in tornadic thunderstorms: The observational evidence. *Mon. Wea. Rev.,* **112,** 2253–2269.

Brooks, H. E., C. A. Doswell, and R. Davies-Jones, 1993: Environmental helicity and the maintenance and evolution of low-level mesocyclones. *The Tornado: Its Structure, Dynamics, Prediction, and Hazards, Geophys. Monogr.,* No. 79, Amer. Geophys. Union, 97–104.

——, ——, and R. B. Wilhelmson, 1994: The role of midtropospheric winds in the evolution and maintenance of low-level mesocyclones. *Mon. Wea. Rev.,* **122,** 126–136.

Brown, R. A., L. R. Lemon, and D. W. Burgess, 1978: Tornado detection by pulsed Doppler radar. *Mon. Wea. Rev.,* **106,** 29–39.

Browning, K. A., and C. R. Landry, 1963: Airflow within a tornadic storm. Preprints, *10th Weather Radar Conf.,* Washington, DC, Amer. Meteor. Soc., 116–122.

Burgess, D. W., V. T. Wood, and R. A. Brown, 1982: Mesocyclone evolution statistics. Preprints, *12th Conf. on Severe Local Storms,* San Antonio, TX, Amer. Meteor. Soc., 422–424.

Cai, H., and R. M. Wakimoto, 2001: Retrieved pressure field and its influence on the propagation of a supercell thunderstorm. *Mon. Wea. Rev.,* **129,** 2695–2713.

Cressman, G. P., 1959: An operational objective analysis system. *Mon. Wea. Rev.,* **87,** 367–374.

Das, P., 1983: Vorticity concentration in the subcloud layers of a rotating cloud. Texas A&M University Rep. for National Science Foundation, 78 pp. [Available from Department of Atmospheric Sciences, Texas A&M University, College Station, TX 77843-3150.]

Davies-Jones, R. P., 1973: The dependence of core radius on swirl ratio in a tornado simulator. *J. Atmos. Sci.,* **30,** 1427–1430.

——, 2000: Can the hook echo instigate tornadogenesis barotropically? Preprints, *20th Conf. on Severe Local Storms,* Orlando, FL, Amer. Meteor. Soc., 269–272.

——, and H. E. Brooks, 1993: Mesocyclogenesis from a theoretical perspective. *The Tornado: Its Structure, Dynamics, Prediction, and Hazards, Geophys. Monogr.,* No. 79, Amer. Geophys. Union, 105–114.

Dowell, D. C., and H. B. Bluestein, 1997: The Arcadia, Oklahoma, storm of 17 May 1981: Analysis of a supercell during tornadogenesis. *Mon. Wea. Rev.,* **125,** 2562–2582.

——, and ——, 2002: The 8 June 1995 McLean, Texas Storm, Part I: Observations of cyclic tornadogenesis. *Mon. Wea. Rev.,* **130,** 2626–2648.

——, ——, and D. P. Jorgensen, 1997: Airborne Doppler radar analysis of supercells during COPS-91. *Mon. Wea. Rev.,* **125,** 365–383.

——, J. Wurman, and L. J. Wicker, 2001: Centrifuging of scatterers in tornadoes. Preprints, *30th Conf. on Radar Meteorology,* Munich, Germany, Amer. Meteor. Soc., 307–309.

Ellis, S., 1997: Hole-filling data voids in meteorological fields. M.S. thesis, School of Meteorology, University of Oklahoma, 198 pp. [Available from School of Meteorology, 100 East Boyd, Norman, OK 73019.]

Fiedler, B. H., 1993: Numerical simulation of axisymmetric tornadogenesis in forced convection. *The Tornado: Its Structure, Dynamics, Prediction, and Hazards, Geophys. Monogr.,* No. 79, Amer. Geophys. Union, 41–48.

Fujita, T. T., 1973: Proposed mechanism of tornado formation from

rotating thunderstorm. Preprints, *Eighth Conf. on Severe Local Storms,* Denver, CO, Amer. Meteor. Soc., 191–196.

——, 1975: New evidence from April 3–4, 1974 tornadoes. Preprints, *Ninth Conf. on Severe Local Storms,* Norman, OK, Amer. Meteor. Soc., 248–255.

——, 1981: Tornadoes and downbursts in the context of generalized planetary scales. *J. Atmos. Sci.,* **38,** 1511–1534.

Heymsfield, G. M., 1978: Kinematic and dynamic aspects of the Harrah tornadic storm analyzed from dual-Doppler radar data. *Mon. Wea. Rev.,* **106,** 233–254.

Hildebrand, P. H., C. A. Walther, C. L. Frush, J. Testud, and F. Baudin, 1994: The ELDORA/ASTRAIA airborne Doppler weather radar: Goals, design, and first field tests. *Proc. IEEE,* **82,** 1873–1890.

Johnson, K. W., P. S. Ray, B. C. Johnson, and R. P. Davies-Jones, 1987: Observations related to the rotational dynamics of the 20 May 1977 tornadic storms. *Mon. Wea. Rev.,* **115,** 2463–2478.

Jorgensen, D. P., T. Matejka, and J. D. DuGranrut, 1996: Multi-beam techniques for deriving wind fields from airborne Doppler radars. *Meteor. Atmos. Phys.,* **59,** 83–104.

Klemp, J. B., 1987: Dynamics of tornadic thunderstorms. *Annu. Rev. Fluid Mech.,* **19,** 369–402.

——, and R. Rotunno, 1983: A study of the tornadic region within a supercell thunderstorm. *J. Atmos. Sci.,* **40,** 359–377.

Lemon, L. R., and C. A. Doswell, 1979: Severe thunderstorm evolution and mesocyclone structure as related to tornadogenesis. *Mon. Wea. Rev.,* **107,** 1184–1197.

Leslie, L. M., 1971: The development of concentrated vortices: A numerical study. *J. Fluid Mech.,* **48,** 1–21.

Lewellen, W. S., 1993: Tornado vortex theory. *The Tornado: Its Structure, Dynamics, Prediction, and Hazards, Geophys. Monogr.,* No. 79, Amer. Geophys. Union, 19–39.

Lilly, D. K., 1982: The development and maintenance of rotation in convective storms. *Intense Atmospheric Vortices,* L. Bengtsson and J. Lighthill, Eds., Springer-Verlag, 149–160.

Markowski, P. M., E. N. Rasmussen, J. M. Straka, and D. C. Dowell, 1998: Observations of low-level baroclinity generated by anvil shadows. *Mon. Wea. Rev.,* **126,** 2942–2958.

NCDC, 1995: *Storm Data.* Vol. 37, No. 6, 178–179.

Rasmussen, E. N., J. M. Straka, R. Davies-Jones, C. A. Doswell, F. H. Carr, M. D. Eilts, and D. R. MacGorman, 1994: Verification of the Origins of Rotation in Tornadoes Experiment: VORTEX. *Bull. Amer. Meteor. Soc.,* **75,** 995–1006.

Ray, P. S., B. C. Johnson, K. W. Johnson, J. S. Bradberry, J. J. Stephens, K. K. Wagner, R. B. Wilhelmson, and J. B. Klemp, 1981: The morphology of several tornadic storms on 20 May 1977. *J. Atmos. Sci.,* **38,** 1643–1663.

Rotunno, R., and J. Klemp, 1985: On the rotation and propagation of simulated supercell thunderstorms. *J. Atmos. Sci.,* **42,** 271–292.

Straka, J. M., E. N. Rasmussen, and S. E. Fredrickson, 1996: A mobile mesonet for finescale meteorological observations. *J. Atmos. Oceanic Technol.,* **13,** 921–936.

Trapp, R. J., and R. Davies-Jones, 1997: Tornadogenesis with and without a dynamic pipe effect. *J. Atmos. Sci.,* **54,** 113–133.

——, E. D. Mitchell, G. A. Tipton, D. W. Effertz, A. I. Watson, D. L. Andra Jr., and M. A. Magsig, 1999: Descending and nondescending tornadic vortex signatures detected by WSR-88Ds. *Wea. Forecasting,* **14,** 625–639.

Wakimoto, R. M., and J. W. Wilson, 1989: Nonsupercell tornadoes. *Mon. Wea. Rev.,* **117,** 1113–1140.

——, and N. T. Atkins, 1996: Observations on the origins of rotation: The Newcastle tornado during VORTEX-94. *Mon. Wea. Rev.,* **124,** 384–407.

——, and H. Cai, 2000: Analysis of a nontornadic storm during VORTEX-95. *Mon. Wea. Rev.,* **128,** 565–592.

——, W.-C. Lee, H. B. Bluestein, C.-H. Liu, and P. H. Hildebrand, 1996: ELDORA observations during VORTEX 95. *Bull. Amer. Meteor. Soc.,* **77,** 1465–1481.

Walko, R. L., 1993: Tornado spin-up beneath a convective cell: Required basic structure of the near-field boundary layer winds. *The Tornado: Its Structure, Dynamics, Prediction, and Hazards, Geophys. Monogr.,* No. 79, Amer. Geophys. Union, 89–95.

Ward, N. B., 1972: The exploration of certain features of tornado dynamics using a laboratory model. *J. Atmos. Sci.,* **29,** 1194–1204.

Weisman, M. L., and J. B. Klemp, 1982: The dependence of numerically simulated convective storms on vertical wind shear and buoyancy. *Mon. Wea. Rev.,* **110,** 504–520.

Wicker, L. J., 1996: The role of near surface wind shear on low-level mesocyclone generation and tornadoes. Preprints, *18th Conf. on Severe Local Storms,* San Francisco, CA, Amer. Meteor. Soc., 115–119.

——, and R. B. Wilhelmson, 1995: Simulation and analysis of tornado development and decay within a three-dimensional supercell thunderstorm. *J. Atmos. Sci.,* **52,** 2675–2703.

Wurman, J., J. M. Straka, and E. N. Rasmussen, 1996: Fine-scale Doppler radar observations of tornadoes. *Science,* **272,** 1774–1777.

——, ——, ——, M. Randall, and A. Zahrai, 1997: Design and deployment of a portable, pencil-beam, pulsed, 3-cm Doppler radar. *J. Atmos. Oceanic Technol.,* **14,** 1502–1512.

Ziegler, C. L., E. N. Rasmussen, T. R. Shepherd, A. I. Watson, and J. M. Straka, 2001: The evolution of low-level rotation in the 29 May 1994 Newcastle–Graham, Texas, storm complex during VORTEX. *Mon. Wea. Rev.,* **129,** 1339–1368.